JOURNAL OF CATALYSIS **178,** 621–639 (1998)
ARTICLE NO. CA982190

# Determination of the Dispersion and Surface Oxidation States of Supported Cu Catalysts

A. Dandekar and M. A. Vannice[1]

*Department of Chemical Engineering, Pennsylvania State University, University Park, Pennsylvania 16802-4400*

Received January 30, 1998; revised June 15, 1998; accepted June 22, 1998

**A combination of CO adsorption at 300 K, which provides irreversible adsorption on $Cu^{+1}$ sites, and oxygen adsorption via $N_2O$ dissociation at 363 K, which counts surface $Cu^0$ atoms, was used to obtain values for the dispersion of Cu on $SiO_2$, $Al_2O_3$, $TiO_2$, $ZrO_2$, diamond powder, and graphitized carbon fibers. The crystallite sizes obtained from these estimates were compared to those obtained from TEM and XRD measurements and were found to be in very good agreement. DRIFT spectra of CO adsorbed on these catalysts were obtained at subambient temperatures as well as at 300 K, and the various amounts of $Cu^0$, $Cu^{+1}$, and $Cu^{+2}$ at the surface were detected by respective peaks in the regions of 2110 $cm^{-1}$ and lower, 2110–2140 $cm^{-1}$, and 2145 $cm^{-1}$ and above. Spectra obtained at 173 K were especially useful because irreversible CO adsorption occurred on all three sites, thus allowing the removal of gas-phase CO and clarifying the spectra of adsorbed CO. Heats of adsorption for CO were determined from the variation in the intensity of the Kubelka–Munk function versus temperature, and the following average values were obtained for Cu dispersed on $SiO_2$, $Al_2O_3$, and diamond: $Cu^0$—4.7 kcal/mole; $Cu^{+1}$—11.7 kcal/mole; and $Cu^{+2}$—5.3 kcal/mole.** 

## INTRODUCTION

Cu catalysts, either supported on an oxide or in the form of a mixed oxide such as copper chromite, have been used in hydrogenation reactions for decades. However, the oxidation states of Cu that are associated with the most active systems are still in dispute, with $Cu^{+1}$ sites being cited as the only active sites in some studies (1–6), whereas the presence of both $Cu^{+1}$ and $Cu^0$ sites have been invoked for optimum activity in other investigations (7–11). Thus the challenge in such studies is not only the determination of the Cu dispersion, which requires the measurement of surface Cu atoms in the form of both metallic atoms and cuprous ions, but also the distribution of the oxidation states among the surface Cu atoms. Measurement of metallic copper surface area is complicated by the weak reversible chemisorption and uncertain adsorption stoichiometries that exist when typical adsorbates such as $H_2$ and CO are used, and the risk of bulk oxidation tends to negate the use of $O_2$ chemisorption (12). As a consequence, dissociative $N_2O$ adsorption according to the stoichiometry at temperatures near 363 K,

$$N_2O_{(g)} + 2\,Cu_s \rightarrow N_{2(g)} + (Cu_2O)_s, \qquad [1]$$

has been the most frequently used technique (13,14). At temperatures around 300 K, which are used to eliminate irreversible CO adsorption on the support (12), CO is easily desorbed from $Cu^0$ and $Cu^{+2}$ sites and it binds irreversibly only with $Cu^{+1}$ species (15–19). CO chemisorption therefore provides the possibility of counting $Cu^{+1}$ sites which, when added to the number of $Cu^0$ sites, could provide a value for the total number of surface Cu atoms (assuming, of course, that no surface $Cu^{+2}$ is present after the reduction step).

In addition to these adsorption studies, numerous investigations of CO adsorption on oxidized and reduced Cu surfaces have been conducted utilizing IR spectroscopy, and peak positions of CO adsorbed on copper have been found to fall in different regions for each oxidation state (19–43). If Cu/zeolite systems are excluded, the reasonable associations that can be made are: $Cu^0$—2110 $cm^{-1}$ and lower; $Cu^{+1}$—2110 to 2140 $cm^{-1}$, and $Cu^{+2}$—2145 $cm^{-1}$ and above (19–37); consequently, IR spectra of adsorbed CO can probe the Cu surface to determine the distribution of oxidation states after a given pretreatment. Although spectra for CO adsorbed on $Cu^0$ and $Cu^{+2}$ sites can be obtained at 300 K under a sufficiently high CO pressure, we have found that subambient spectra acquired with a modified DRIFTS cell in the absence of gas-phase CO represent higher coverages and provide more well defined peaks. Thus we have combined this approach with CO adsorption and $N_2O$ decomposition measurements as well as additional characterization by TEM and XRD to examine Cu dispersed on $SiO_2$, $\eta$-$Al_2O_3$, $TiO_2$, $ZrO_2$, synthetic diamond powder and graphitized carbon fibers. This paper describes the results related to Cu dispersion (hence, Cu and Cu oxide crystallite sizes) and the oxidation state of the surface Cu atoms after a variety of pretreatments.

[1] Corresponding author.



0021-9517/98 $25.00

## EXPERIMENTAL

The support materials used in this study were 60/120 mesh cuts of $SiO_2$ (Grade 57, Davison Chemical Co.), $\eta$-$Al_2O_3$ (prepared by calcining $\beta$-aluminum trihydrate at 873 K for 5 h), $TiO_2$ (P-25, Degussa Co.), $ZrO_2$ (Alfa Aesar), synthetic diamond powder (Alfa Aesar), designated DM, and Tornel P-25 pitch-based graphitized carbon fibers, designated GF. All catalysts contained appropriately 5 wt% Cu and were prepared with an impregnation technique using $Cu(NO_3)_2$ dissolved in the following respective amounts of distilled deionized water for the six supports just mentioned: 0.6, 0.6, 0.5, 0.4, 0.3, and 0.3 ml/g. Prior to characterization, the catalyst samples were pretreated *in situ* in flowing He or Ar for 1 h at a given temperature, then reduced in flowing $H_2$ or calcined in 20% $O_2$/80% Ar at the same temperature for 4 h. Typical space velocities were 20000 $h^{-1}$.

Oxygen chemisorption via dissociative $N_2O$ adsorption at 363 K was used to count metallic Cu surface atoms. The measurements were carried out in a P-E TGA system with a sensitivity of 0.1 $\mu$g. After loading a sample in the analyzer pan, it was pretreated *in situ* at either 473 or 573 K under $H_2$ before cooling to 363 K. Using mass flow controllers (Tylan, Model FC-260), $N_2O$ (99.999%, Matheson) was introduced at 75 Torr (balance Ar) and the increase in weight was monitored until it asymptotically reached a steady-state value. The sample was then purged with Ar (99.999%, MG Ind.) to remove the reversibly adsorbed $N_2O$. The difference between the final and the initial weights of the sample represents the oxygen required to oxidize the surface $Cu^0$ atoms to form $(Cu_2O)_s$ according to Eq. [1].

After a chosen pretreatment under $H_2$ at either 473 or 573 K, CO uptakes on the catalyst sample were measured at 300 K in a stainless steel volumetric adsorption system giving a vacuum below $10^{-6}$ Torr at the sample (11). Following the initial isotherm, the sample was evacuated for 1 h at 300 K and a second isotherm was measured to determine reversible adsorption. The irreversible adsorption obtained from the difference between the two isotherms was attributed to CO adsorbed only on $Cu^{+1}$ sites (15–19). The $H_2$ (99.999%, MG Ind.) and CO (99.99% Matheson) were flowed through separate molecular sieve traps (Supelco) and Oxytraps (Alltech Assoc.) for additional purification. Oxygen and CO uptakes on the catalysts were also determined after subjecting a sample of each catalyst to the following pretreatment: heat in He or Ar to 573 K and hold at 573 K for 1 h, reduce in $H_2$ for 4 h at 573 K, purge with He or Ar at 573 K for 30 min, cool to 363 K, expose to 10% $N_2O$ in He or Ar at 363 K for 30 min to convert all metallic Cu on the surface to $Cu_2O$ (14), and finally purge in Ar or evacuate at 363 K for 30 min. Following this sequence of *in situ* steps , either the oxygen (O) uptake at 363 K or the CO uptake at 300 K was measured on these samples according to the procedures outlined previously.

The XRD spectra were obtained *ex situ* using a Rigaku Geigerflex diffractometer equipped with a $CuK_a$ radiation source and a graphite monochromator. After the desired pretreatment, each sample was passivated by exposure to a flowing mixture of 1% $O_2$ in He for 1 h at 300 K prior to the XRD measurements, which were made in air. The passivated samples were also examined in a Philips 420T transmission electron microscope, operated at a high tension voltage of 120 KV, after they were ultrasonically dispersed in acetone and placed on a 400-mesh, carbon-coated copper grid. Typically 120 to 150 particles were counted for each catalyst to determine particle size distributions.

The infrared studies were conducted with a Sirius 100 FTIR system (Mattson Instr., Inc.) using a DRIFTS cell (HVC-DPR, Harrick Sci. Corp.) that has been extensively modified to allow *in situ* treatments up to 800 K under flowing gases. An inexpensive stainless steel device utilizing a solenoid valve and temperature controller was used to cool the reactor cell to subambient temperatures with liquid nitrogen (44). Details of the cell modification and the data acquisition and handling procedures have been given previously (44–46). After loading the sample powder into the DRIFTS cell (ca. 50–80 mg), a standard procedure was used to collect the interferograms. The first obtained was that of the initial untreated sample at 300 K under flowing Ar (20 $cm^3$/min). Following this, the sample was subjected to the desired *in situ* pretreatment procedure. To maximize $Cu^{+2}$ formation, samples of $Cu/SiO_2$ and $Cu/Al_2O_3$ were calcined in 20% $O_2$/80% Ar at 573 K, whereas the Cu/DM catalyst was calcined at 423 K under similar conditions. To study reduced samples, each catalyst was pretreated *in situ* at either 423, 473, 573, or 673 K in flowing $H_2$. After the chosen pretreatment, each sample was cooled to 300 K to collect an interferogram, which was used as the background reference for subsequent spectra of that sample. Following this, the catalyst was exposed to a flowing mixture of 10% CO and 90% Ar at 300 K for 30 min, then another interferogram was collected under 75 Torr CO. The sample was then purged with pure Ar for 30 min and the last interferogram was obtained. All these spectra were obtained at 300 K. If spectra at subambient temperatures were desired, the heating cartridge was then replaced with the cooling device and the sample holder was cooled to a temperature between 273 K and 148 K. After stabilizing the temperature at the desired value, a flowing mixture of 10% CO in Ar was reintroduced to the DRIFTS cell for 30 min, then the sample was purged with Ar for 30 min before collecting the interferogram at that temperature. The temperature was further reduced, the sample was exposed again to 10% CO in Ar before purging for 30 min, and another interferogram was collected. This procedure was followed down to 148 K. These interferograms, when Fourier transformed using the interferogram of the corresponding pretreated catalyst at 300 K prior to CO exposure as a reference, yielded the

Kubelka–Munk or absorbance spectrum for CO adsorbed on the catalyst at each adsorption temperature. All samples were analyzed without a diluent except for the Cu/GF sample, which was diluted with $CaF_2$ in a 5 : 1 diluent : sample weight ratio to enhance the signal-to-noise ratio.

## RESULTS

Table 1 lists the irreversible CO uptakes on Cu/DM, $Cu/SiO_2$, $Cu/Al_2O_3$, and $Cu/TiO_2$ after reduction at either 473 or 573 K, and the amounts of oxygen chemisorbed on these catalysts after similar pretreatments, calculated from $N_2O$ decomposition, are also listed. A typical set of isotherms is shown in Fig. 1 representing CO adsorption on $Cu/Al_2O_3$. Figure 2 shows the corresponding weight gain versus time plots for $N_2O$ decomposition on $Cu/Al_2O_3$ which demonstrate the initial weight gain due to oxygen uptake and $N_2O$ adsorption as well as the weight loss after purging with Ar to remove adsorbed $N_2O$. As seen in Table 1, the irreversible CO uptake for each of the catalysts drops significantly as the reduction temperature is increased from 473 to 573 K. In contrast, the amount of $N_2O$ decomposed on these catalysts significantly increases as the reduction temperature is increased from 473 to 573 K. Assuming a stoichiometry of $O : Cu_s^0 = 1 : 2$ for metallic Cu sites and $CO : Cu_s^{+1} = 1$ for cuprous ion sites, Cu dispersions ($D = Cu_{surf}/Cu_{total}$) were calculated and are given in Table 1. The $Cu^0$ crystallite size, d, based on $O_{(ad)}$ was obtained using the equation $d\ (nm) = 1.1/D$ (12–14), while $Cu_2O$ crystallite sizes were estimated from the CO uptake using the relation $d\ (nm) = 1.2/D$ derived on the assumption of a $Cu^{+1}$ site density of $5.2 \times 10^{18}\ m^{-2}$ (47), a value in excellent agreement with UHV results reported by Pritchard and co-workers (24). These values are listed in Table 2. As an approximation of crystallite sizes based on the sum of the O and CO uptakes, the relation $d\ (nm) = 1.15/D$ was used.

**TABLE 1**

**Irreversible Gas Uptakes and K-M Intensities for CO Adsorption on $Cu^{+1}$ at 300 K**

| Catalyst | $T_{RED}$ (K) | Irreversible uptakes: CO[a] ($\mu$mol/g) | Irreversible uptakes: Oxygen ($\mu$mol O/g) | Cu dispersion $[(Cu_s^0 + Cu_s^{+1})/Cu_{Total}]$ | KM intensity |
|---|---|---|---|---|---|
| 5% Cu/DM | 473 | 45 | 19 | 0.10 | 0.0036 |
| 5% Cu/DM | 573 | 35 | 25 | 0.11 | 0.0028 |
| 5% Cu/DM[b] | 573 | 83 | 0 | 0.10 | 0.008 |
| 5.1% $Cu/SiO_2$ | 473 | 58 | 36 | 0.16 | 0.0188 |
| 5.1% $Cu/SiO_2$ | 573 | 18 | 86 | 0.24 | 0.005 |
| 5.1% $Cu/SiO_2$[b] | 573 | 162 | 0 | 0.2 | 0.058 |
| 4.9% $Cu/Al_2O_3$ | 473 | 60 | 168 | 0.52 | 0.05 |
| 4.9% $Cu/Al_2O_3$ | 573 | 10 | 354 | 0.93 | 0.008 |
| 4.9% $Cu/Al_2O_3$[b] | 573 | 382 | 0 | 0.5 | 0.32 |
| 4.9% $Cu/TiO_2$ | 473 | 4 | 248 | 0.65 | 0.0025 |
| 4.9% $Cu/TiO_2$ | 573 | 0 | 270 | 0.7 | 0 |
| 4.9% $Cu/TiO_2$[b] | 573 | 410 | 0 | 0.53 | 0.31 |
| 5.2% $Cu/ZrO_2$[b] | 573 | 51 | 0 | 0.014 | 0.0075 |
| 5.1% Cu/GF[b] | 573 | 7 | 0 | 0.009 | 0.0005 |

[a] At 75 Torr CO pressure.

[b] Exposed to 75 Torr $N_2O$ for 30 min @ 363 K following the treatment in $H_2$.

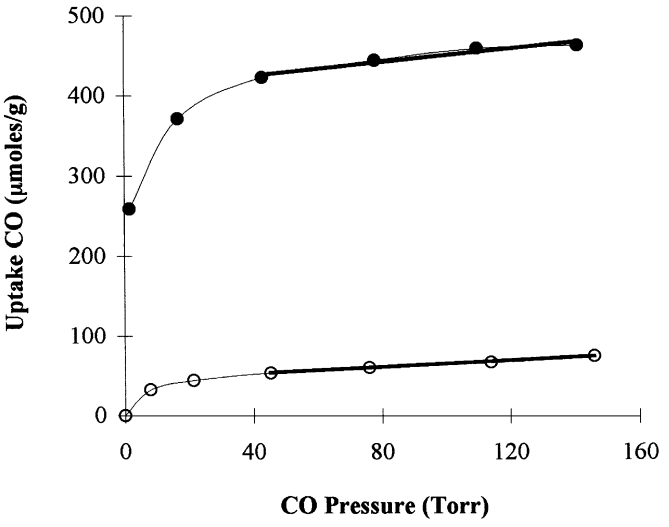


**FIG. 1.** CO adsorption isotherms for 4.9% Cu/$\eta$-$Al_2O_3$ reduced at 573 K after exposure to $N_2O$ at 363 K; filled circles: total uptake; open circles: reversible uptake.

Surface- and volume-averaged Cu particle sizes for Cu/DM, $Cu/SiO_2$, $Cu/Al_2O_3$, and $Cu/TiO_2$, obtained from the TEM micrographs of these catalysts after reduction at either 473 or 573 K, are also listed in Table 2, along with those calculated from the line widths of the XRD patterns using the Scherrer equation. Crystallite sizes calculated from the line widths of both the $Cu_2O$ and the Cu peaks after pretreatments at 473 and 573 K are listed. The XRD patterns for $Cu/Al_2O_3$ and $Cu/TiO_2$ exhibited no detectable signals corresponding to either of the two expected copper phases after either of the reduction pretreatments. This is consistent with the information from TEM which indicates the presence of only very small Cu (or Cu oxide) particles which would give broad peaks difficult to detect in the X-ray patterns. In the case of Cu/DM, the strong reflection at $2\theta = 43.7^\circ$, characteristic of the diamond lattice structure, coincides with the primary signal from metallic Cu; consequently, the secondary $Cu^0$ reflection at $2\theta = 50.1^\circ$ was used to estimate Cu crystallite in this catalyst.

Figure 3 shows the Kubelka–Munk (K-M) IR spectra (defined later) of CO adsorbed on the $Cu/SiO_2$ sample after exposure to 75 Torr CO followed by purging with Ar. The bands remaining in the spectra after purging represent CO species strongly bound on the Cu or Cu oxide sites present. As illustrated by Fig. 3A, $Cu/SiO_2$ reduced at 473 K exhibits a strong absorption peak at 2120 $cm^{-1}$. After reduction at 573 K, this peak essentially disappears leaving another very

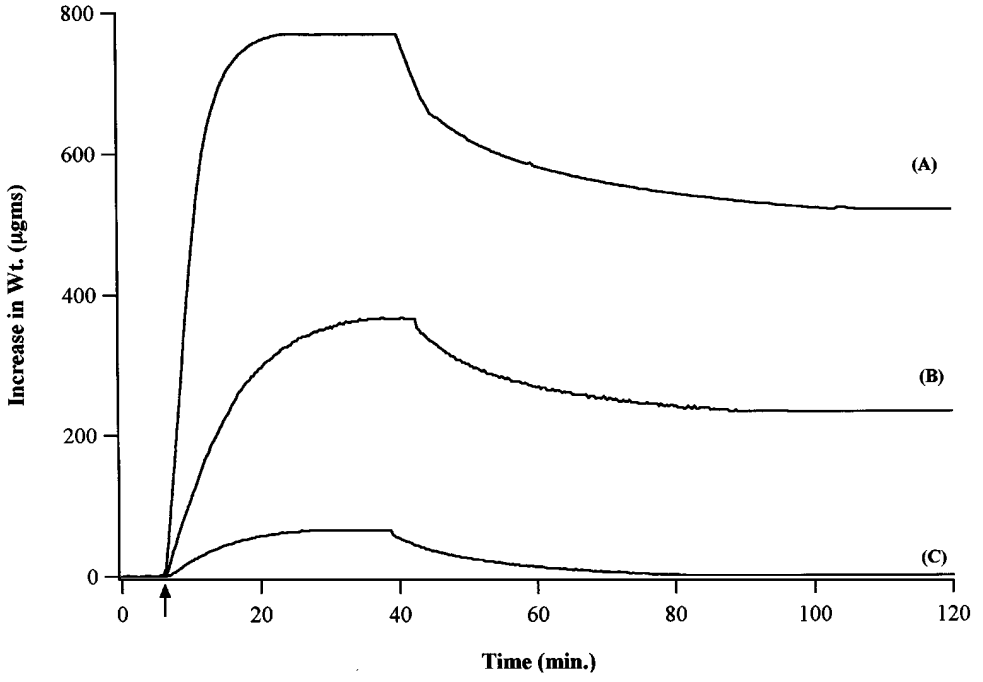


**FIG. 2.** Weight change during $N_2O$ decomposition at 363 K on 5% $Cu/Al_2O_3$ after reduction at: (A) 575 K, (B) 473 K. Arrow denotes introduction of 10% $N_2O$ in Ar. Purging was initiated at 40 min; (C) pure $Al_2O_3$.

weak peak at 2105 $cm^{-1}$. Conversion of the Cu surface to $Cu_2O$ markedly increases the 2120 $cm^{-1}$ peak intensity. Similar spectra for $Cu/Al_2O_3$, $Cu/TiO_2$, and Cu/DM are shown in Figs. 4, 5, and 6, respectively. The spectrum of $Cu/Al_2O_3$ reduced at 473 K (Fig. 4A) exhibits a sharp absorption peak at 2111 $cm^{-1}$ whose intensity drops considerably after the reduction at 573 K (Fig. 4B). A comparison of the spectra in 4a and 4b demonstrates the strong similarity between the K-M and Absorbance scales. The spectra for $Cu/TiO_2$ (Fig. 5) exhibit very weak bands around 2100 $cm^{-1}$ and 2020 $cm^{-1}$ after either reduction pretreatment. Figure 6 shows the spectra of the Cu/DM catalyst after each reduction pretreatment. Similar to $Cu/SiO_2$ and $Cu/Al_2O_3$, reduction at 473 K gives a distinct band at 2118 $cm^{-1}$; however, a weak band around 2160 $cm^{-1}$ is also evident. As the reduction temperature is increased to 573 K, there is a sharp decrease in the 2118 $cm^{-1}$ band intensity and the other band essentially disappears. Again, though, oxidation of the surface to $Cu_2O$ greatly enhances the 2118 $cm^{-1}$ peak. Figure 7 shows DRIFTS spectra for CO adsorbed on the $Cu/ZrO_2$

**TABLE 2**

**Comparison of Average Cu Crystallite Sizes (in nm)**

| Catalyst | $T_{RED}$ (K) | Based on CO[a] ($Cu^{+1}$) | Based on O uptake[b] ($Cu^0$) | Based on (O + CO) uptakes[c] ($Cu^0 + Cu^{+1}$) | TEM $d_s$ | TEM $d_r$ | XRD $Cu_2O$ | XRD Cu |
|---|---|---|---|---|---|---|---|---|
| 5% Cu/DM | 473 | 20 | 23 | 11 | 15 | 19 | 13 | 17[e] |
| 5% Cu/DM | 573 | 27 | 18 | 10 | 13 | 22 | 12 | 14[e] |
| 5.1% $Cu/SiO_2$ | 473 | 16 | 12 | 7 | 6 | 9 | 2 | 5 |
| 5.1% $Cu/SiO_2$ | 573 | 54 | 5 | 5 | 5 | 8 | ND | 5.1 |
| 4.9% $Cu/Al_2O_3$ | 473 | 15 | 3 | 2 | ND | ND | ND | ND |
| 4.9% $Cu/Al_2O_3$ | 573 | 92 | 1 | 1 | ND | ND | ND | ND |
| 4.9% $Cu/TiO_2$ | 473 | 231 | 2 | 2 | 2 | 3 | ND | ND |
| 4.9% $Cu/TiO_2$ | 573 | ND[d] | 2 | 2 | 2 | 3 | ND | ND |

[a] Based on D = 1.2/d (nm) for $Cu_2O$ (Ref. 47).
[b] Based on D = 1.1/d (nm) for $Cu^0$ (Refs. 12–14).
[c] Based on an average relationship of D = 1.15/d (nm).
[d] ND = not detectable.
[e] Estimated from secondary $Cu^0$ reflection at $2\theta = 50.1°$.

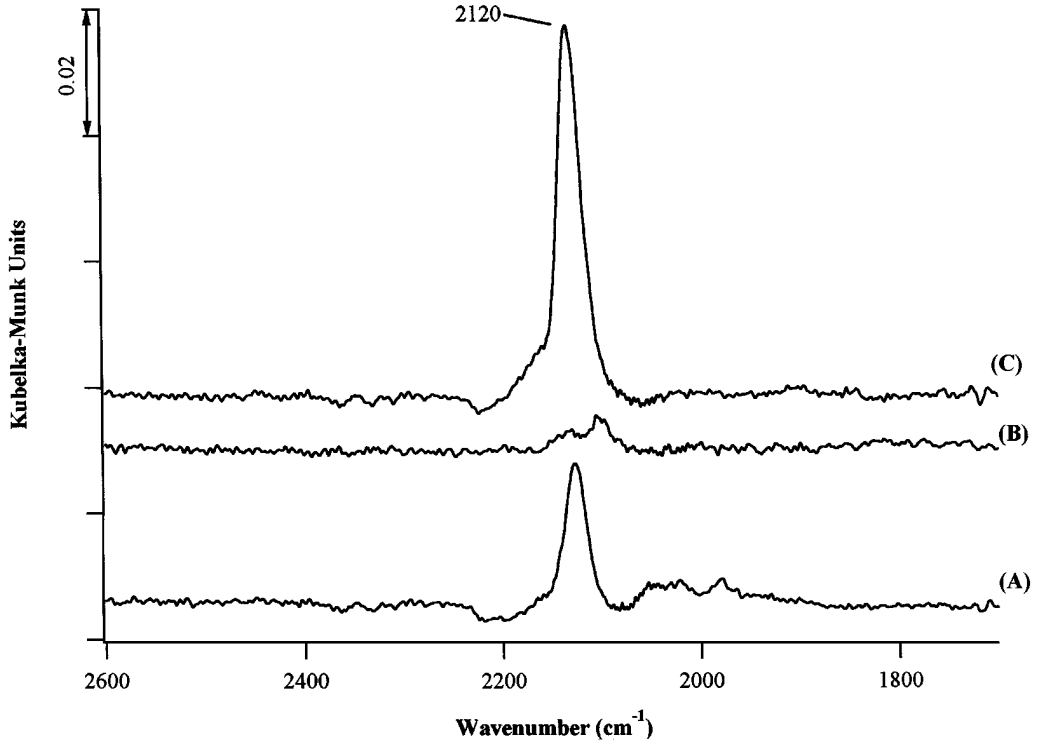


**FIG. 3.** DRIFTS spectra of CO adsorbed at 300 K on 5.1% $Cu/SiO_2$: (A) reduced at 473 K, (B) reduced at 573 K, (C) reduced at 573 K and reoxidized under 75 Torr $N_2O$ at 363 K; $P_{CO} = 75$ Torr, then 1-h purge with Ar.

and Cu/GF samples after reduction at 573 K followed by exposure to 150 Torr $N_2O$ at 363 K to oxidize the Cu surface to $Cu_2O$.

DRIFT spectra collected at subambient temperatures are shown in the next set of figures, i.e., Figs. 8–16. Compared to the K-M function, the absorbance scale is much more sensitive towards detecting very weak peaks, which appeared in certain spectra collected at subambient temperatures; however, to date only K-M intensities of DRIFT spectra have been quantitatively related to surface concentrations. Consequently, to allow the detection of these weak peaks, the absorbance scale was chosen to represent the spectra of $Cu/SiO_2$ whereas all other spectra are represented by the K-M function. Figure 8 shows spectra of CO adsorbed at different temperatures on 5% $Cu/SiO_2$ after calcination at 573 K, while corresponding spectra after reduction at 473 and 573 K are shown in Figs. 9 and 10, respectively. As illustrated in Fig. 8, no detectable bands exist at 300 K, indicating the absence of any strongly bound CO species after purging. At 273 K, a weak peak is observed at 2155 $cm^{-1}$ whose intensity increases as the adsorption temperature decreases, and the peak position shifts to 2159 $cm^{-1}$ at 148 K. At temperatures of 223 K and lower, a distinct shoulder develops at 2130 $cm^{-1}$ along with a very weak broad band around 2240 $cm^{-1}$. In contrast, irreversible CO adsorption occurs at 300 K on the catalyst reduced at 473 K and produces a distinct stable band at 2115 $cm^{-1}$, as observed in Fig. 9. As the adsorption temperature decreases, this band intensity steadily increases and a small shift in wavenumber to 2117 $cm^{-1}$ occurs. A weak shoulder around 2149 $cm^{-1}$ can also be seen below 223 K. Reduction at 573 K entirely removes the strong residual band at 2115 $cm^{-1}$ observed in the previous spectrum at 300 K, as demonstrated in Fig. 10. At lower temperatures, bands develop at 2101 and 2062 $cm^{-1}$, with the former band developing into a very strong band at 2107 $cm^{-1}$ at 148 K, while a new shoulder is detected near 2160 $cm^{-1}$.

Similar spectra for CO adsorbed on 5% $Cu/Al_2O_3$ first calcined at 573 K and then reduced at either 473 or 573 K are shown in Figs. 11–13, respectively. The spectrum of the calcined sample at 300 K again exhibits no features, whereas the samples reduced at 473 K or 573 K exhibit stable bands at 2112 and 2105 $cm^{-1}$, respectively. As the adsorption temperature is progressively lowered, one predominant peak develops at 2158 $cm^{-1}$ for the calcined sample, while with the catalyst reduced at 473 K, the peak at 2112 $cm^{-1}$ grows and shifts to 2127 $cm^{-1}$. With the catalyst reduced at 573 K, the band at 2105 $cm^{-1}$ grows and shifts to 2099 $cm^{-1}$ as the temperature decreases, while additional bands develop at 2003 and 2108 $cm^{-1}$.

The additional features that develop as the temperature is lowered are clearly evident, and they are optimized at the lowest temperatures achieved here, i.e., 148 or 173 K. Consequently, the effect of reduction temperature on the

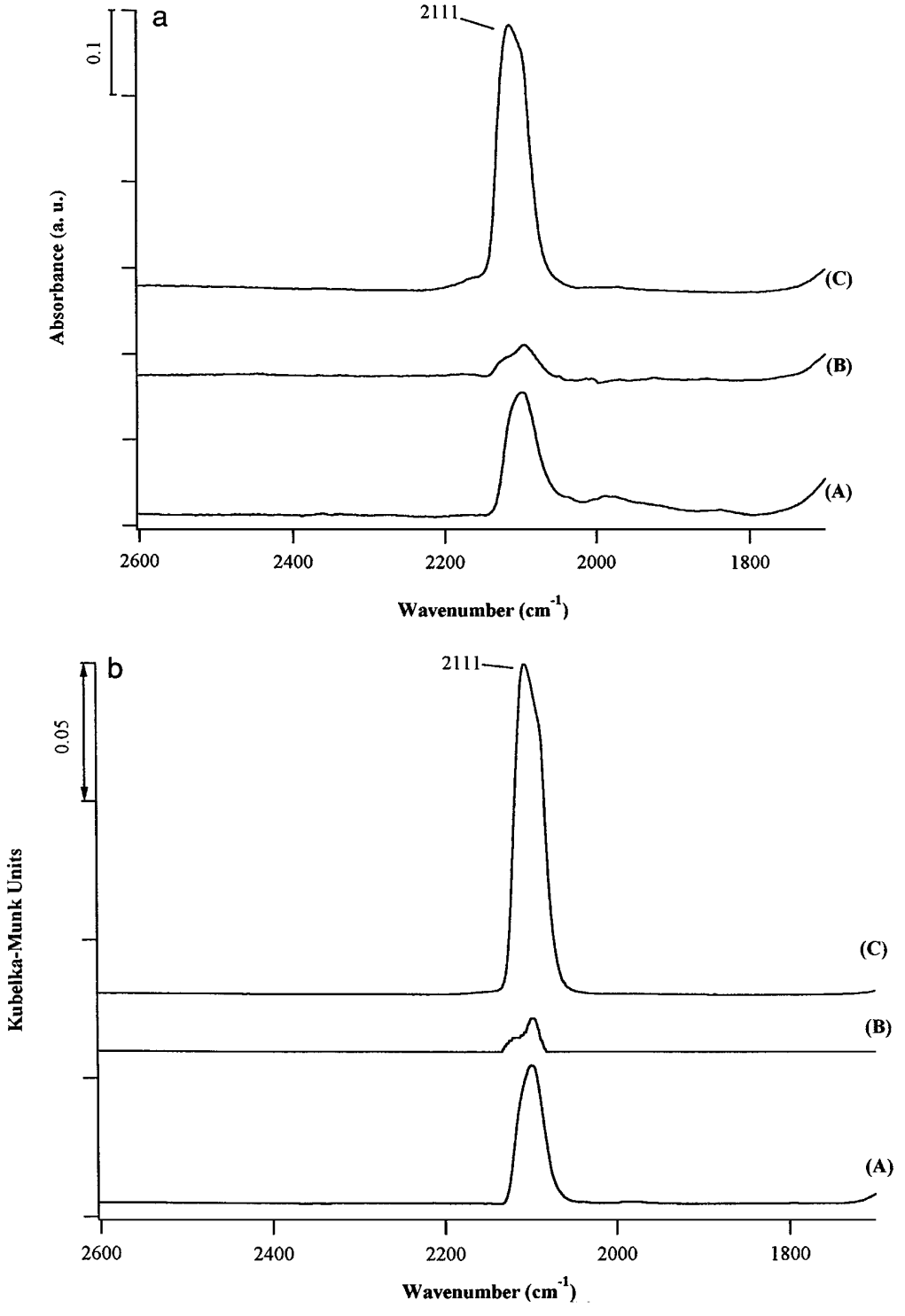


**FIG. 4.** DRIFTS spectra of CO adsorbed at 300 K on 4.9% $Cu/Al_2O_3$: (A) reduced at 473 K, (B) reduced at 573 K, (C) reduced at 573 K and reoxidized under 75 Torr $N_2O$ at 363 K; $P_{CO} = 75$ Torr.

presence of different adsorption sites on these Cu catalysts can be readily examined by obtaining a single spectrum at 148 or 173 K, and the results of this approach are illustrated in Fig. 14 for Cu/DM and in Fig. 15 for Cu/GF. A low temperature calcination produces two peaks at 2158 and 2120 $cm^{-1}$ for the Cu/DM sample with the former band disappearing as the reduction temperature increases to 473 K to leave a dominant single band at 2130 $cm^{-1}$. Reduction

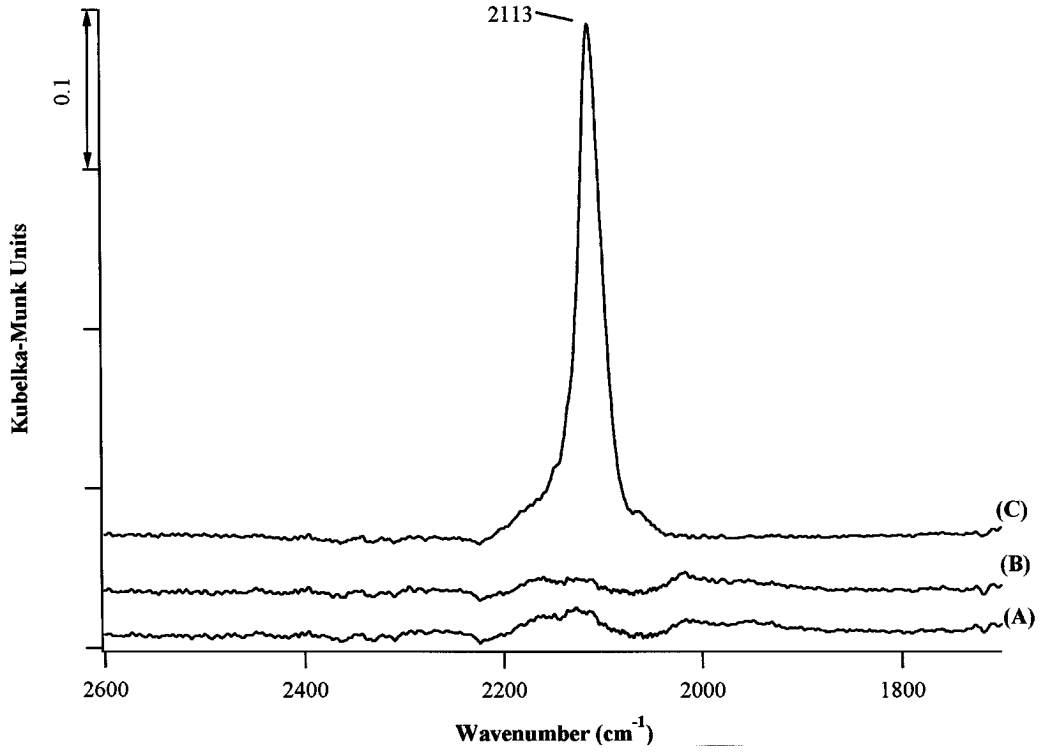


**FIG. 5.** DRIFTS spectra of CO adsorbed at 300 K on 4.9% $Cu/TIO_2$: (A) reduced at 473 K, (B) reduced at 573 K, (C) reduced at 573 K and reoxidized under 75 Torr $N_2O$ at 363 K; $P_{CO} = 75$ Torr.

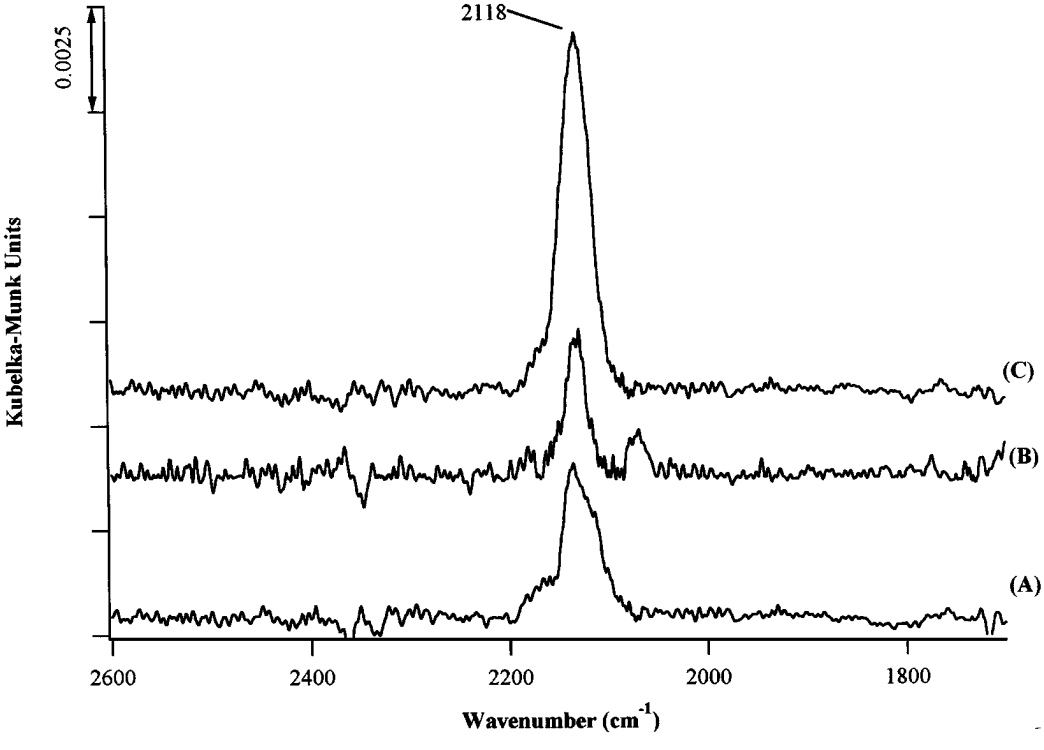


**FIG. 6.** DRIFTS spectra of CO adsorbed at 300 K on 5% Cu/DM: (A) reduced at 473 K, (B) reduced at 573 K, (C) reduced at 573 K and reoxidized under 75 Torr $N_2O$ at 363 K; $P_{CO} = 75$ Torr.

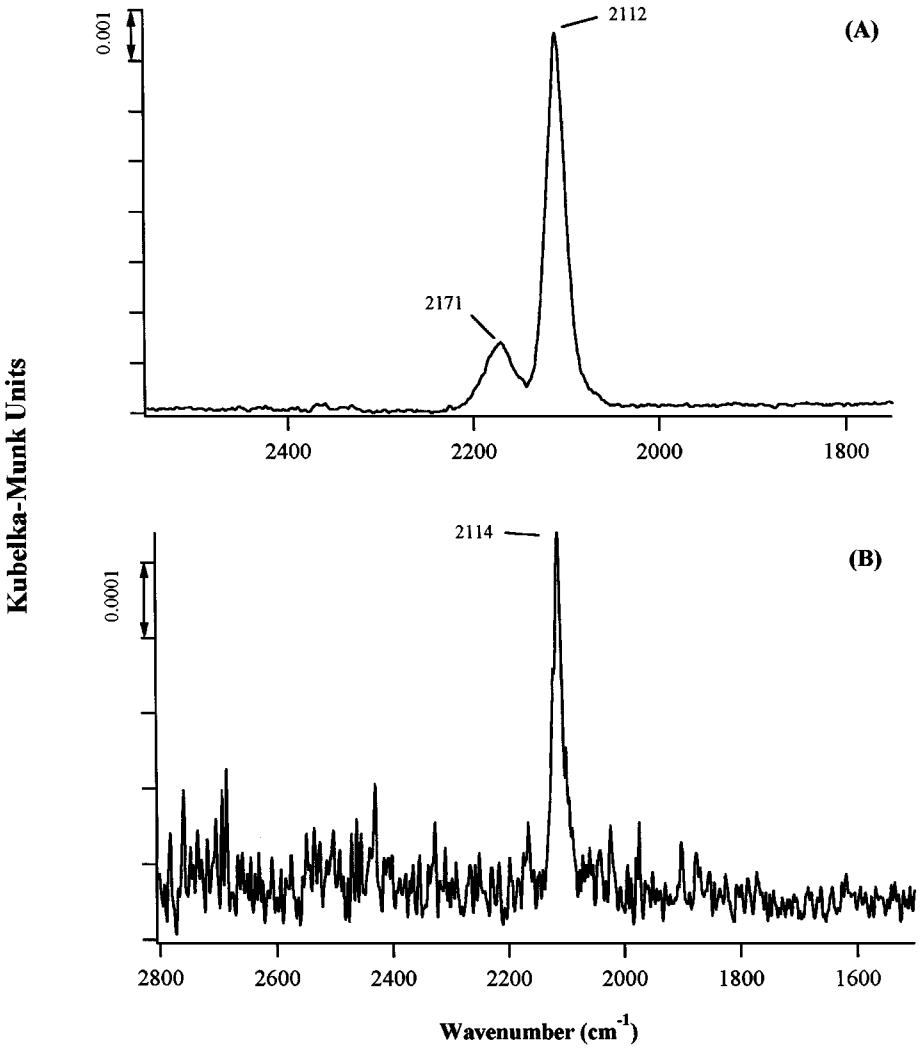


**FIG. 7.** DRIFTS spectra of CO adsorbed at 300 K on (A) 5.2% $Cu/ZrO_2$ and (B) 5.1% Cu/GF following reduction at 573 K and reoxidation to $Cu_2O$ under 75 Torr $N_2O$ at 363 K; $P_{CO} = 75$ Torr.

at 573 K decreases the peak intensity at 2130 $cm^{-1}$ and causes a peak at 2110 $cm^{-1}$ to develop, which becomes the dominant peak after reduction at 673 K. In similar fashion, two peaks at 2155 and 2122 $cm^{-1}$ are detected for the Cu/GF sample after heating the impregnated sample in Ar at 423 K. As the reduction temperature increases, the 2155 $cm^{-1}$ band disappears and a band at 2092 $cm^{-1}$ develops. Only the latter band is observed after reduction at 673 K, as shown in Fig. 15.

## DISCUSSION

Adsorption of CO on copper surfaces in different oxidation states has been shown to give rise to various species which exhibit IR absorption bands in the 2000–2200 $cm^{-1}$ spectral region as well as between 1200–1700 $cm^{-1}$ (19). Bands in the former region have been associated with linear or bridge-bonded CO interacting with sites on either CuO, $Cu_2O$, or $Cu^0$ surfaces. Although disagreement exists regarding assignment of bands to the precise Cu oxidation state, especially in the older literature, some assignment rules have been unanimously agreed upon: (1) $Cu^{+2}$-CO species will absorb at a frequency higher than that at which a corresponding $Cu^{+1}$-CO species will absorb, while a $Cu^0$-CO species will absorb at a lower frequency than for $Cu^{+1}$-CO species; (2) a bridged carbonyl species will absorb at lower wavenumbers than a linear carbonyl species; and (3) adsorption on $Cu^{+2}$ and $Cu^0$ sites is predominantly weak and reversible at 300 K and higher (21–37). In general, absorption above 2140 $cm^{-1}$ has been associated with $Cu^{+2}$ sites, and Busca has presented arguments why the wavenumber should be higher than that of gas-phase CO (28). In contrast, weakly bound CO on metallic Cu has been shown to manifest stretching frequencies typically below 2110 $cm^{-1}$. CO binds most strongly on $Cu^{+1}$ sites, and bands for these species have repeatedly been reported between

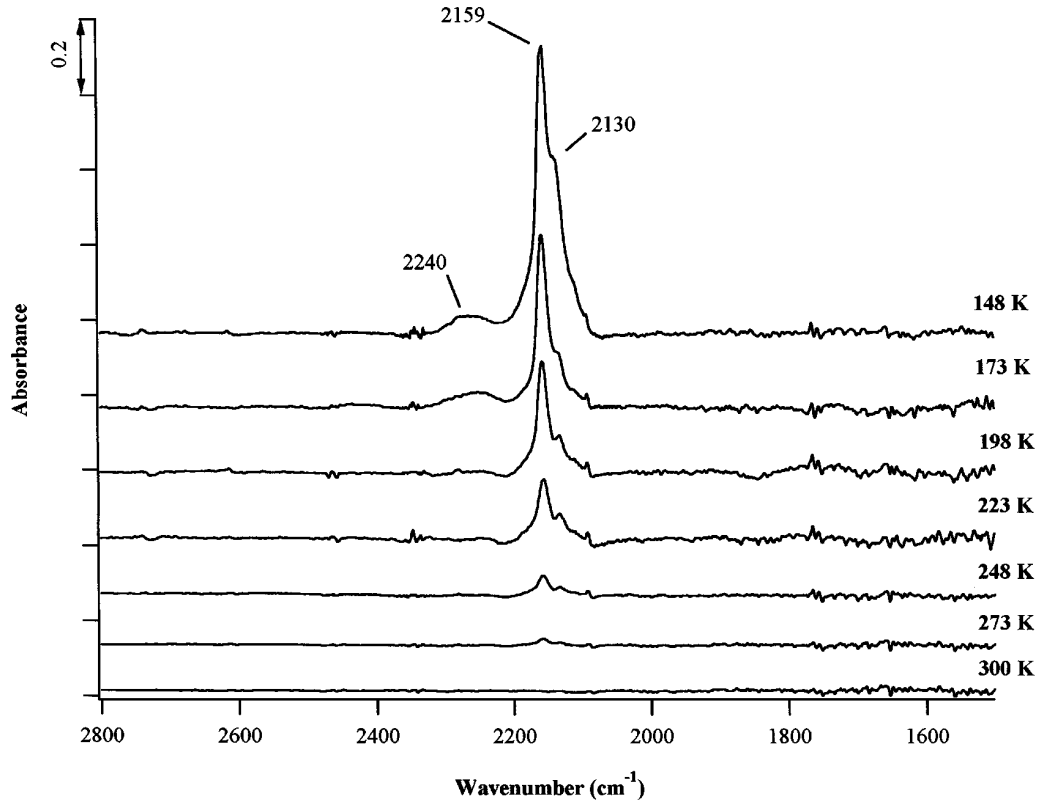


**FIG. 8.** DRIFT spectra of CO adsorbed at different temperatures on 5.1% $Cu/SiO_2$ calcined at 573 K. Each spectrum taken after exposure to 75 Torr CO and a 30-min purge in Ar.

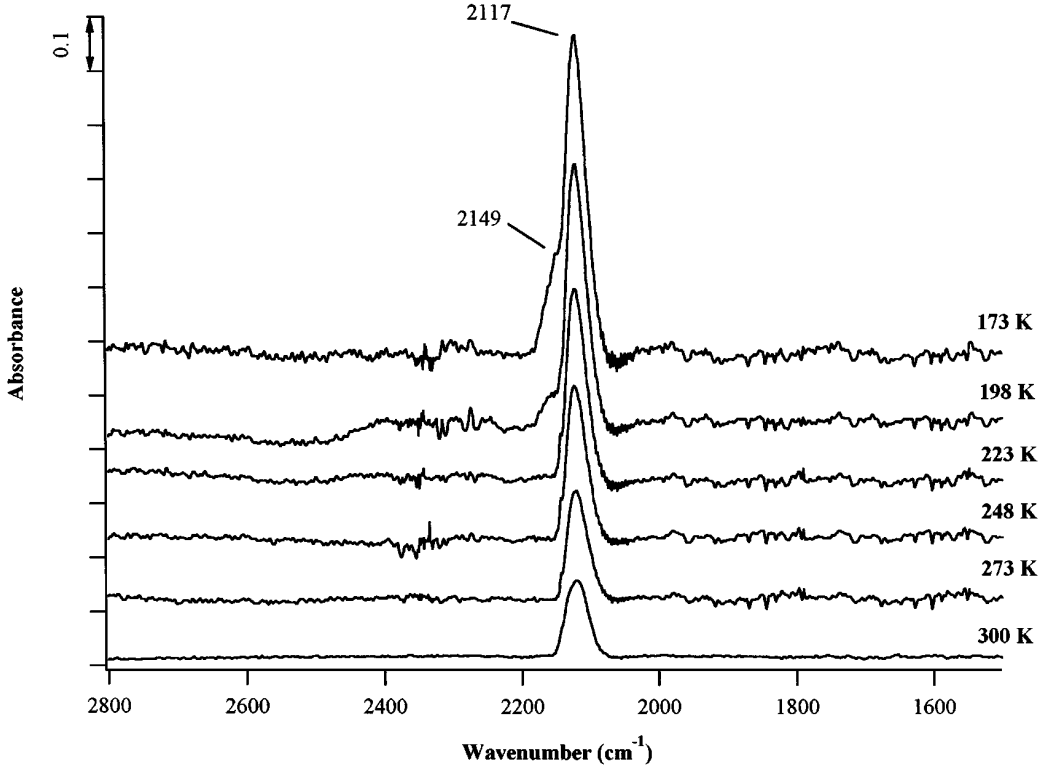


**FIG. 9.** DRIFT spectra of CO adsorbed at different temperatures on 5.1% $Cu/SiO_2$ reduced at 473 K.

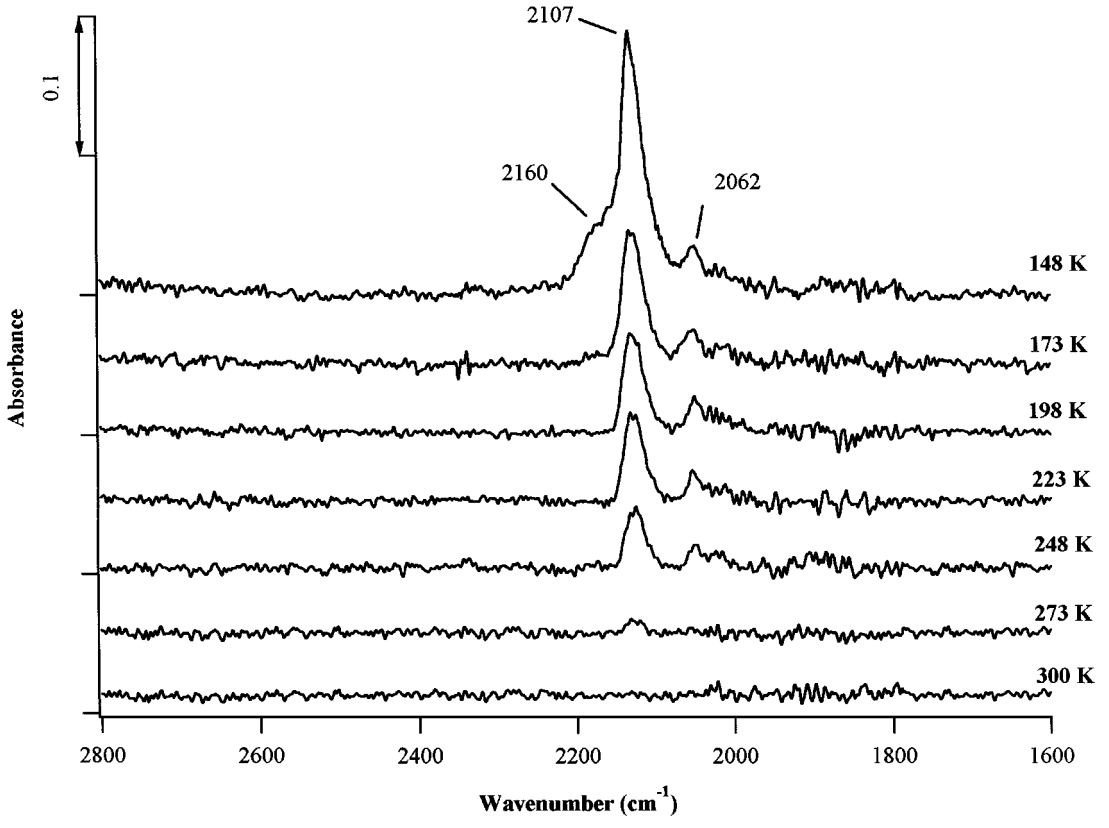


**FIG. 10.** DRIFT spectra of CO adsorbed at different temperatures on 5.1% $Cu/SiO_2$ reduced at 573 K.

2110 and 2135 $cm^{-1}$, as illustrated in Table 3. Consequently, bands near 2110 $cm^{-1}$ have the potential to represent either $Cu^{+1}$-CO or $Cu^0$-CO species; however, the adsorption strength provides a method to distinguish between CO adsorbed on these two surfaces. Both the correlation of the wavenumber regions with CO adsorbed on the three oxidation states of Cu and the relative binding strengths have been explained by considering the $\pi$-acceptor and $\sigma$-donor properties of the CO molecule (19).

Unfortunately, these previous studies did not use additional characterizational techniques to confirm the oxidation state of the Cu species present, hence the reason for the numerous disparities in assignments. Surprisingly, not even the relative thermal stability of the $Cu^{+1}$-CO species has been used to verify its assignment. Based upon this information, differences in the stability of adsorbed CO species as well as their peak position can be used to verify band assignments. Therefore, the strong 2120 $cm^{-1}$ peak at 300 K in the spectrum of $Cu/SiO_2$ reduced at 473 K can be unambiguously attributed to CO linearly bonded with surface $Cu^{+1}$ sites. After reduction at 573 K, the band completely disappears, indicating reduction of the remaining cuprous oxide. Similarly, the irreversibly adsorbed CO providing a peak between 2111 and 2118 $cm^{-1}$ at 300 K in the spectra of Cu dispersed on $Al_2O_3$, $TiO_2$, and DM can be associated with linear $Cu^{+1}$-CO species.

**TABLE 3**

**Infrared Band Positions for CO Adsorbed on Supported Cu**

| Support | Adsorption site | Frequency ($cm^{-1}$) | Reference |
|---|---|---|---|
| $SiO_2$ | $Cu^0$ | 2100–2110 | (21) |
| | | 2079-2101 | (23) |
| | | 2110 | (27) |
| | | 2090-2113 | (29) |
| | $Cu^{+1}$ | 2118 | (29) |
| | | 2126 | (34) |
| | | 2115-2130 | (35–37) |
| | $Cu^{+2}$ | 2140-2240 | (25,26) |
| | | 2180,2199,2216 | (34) |
| $Al_2O_3$ | $Cu^0$ | 2100-2110 | (21) |
| | | 2110 | (27) |
| | | 2100 | (32) |
| | | 2102,2094,2087 | (31) |
| | $Cu^{+1}$ | 2115,2130-2135,2140 | (19) |
| | | 2118 | (30) |
| | | 2115,2120,2135 | (32) |
| $TiO_2$ | $Cu^0$ | 2103,2071 | (33) |
| | $Cu^{+1}$ | 2128 | (33) |
| $ZrO_2$ | $Cu^0$ | 2110,2105,2100 | (32) |
| | $Cu^{+1}$ | 2120-2130 | (32) |
| ZnO | $Cu^0$ | 2065-2078,2090 | (33) |
| MgO | $Cu^0$ | 2081-2083 | (21) |
| Unsupported CuO | $Cu^{+2}$ | 2158 | 28 |

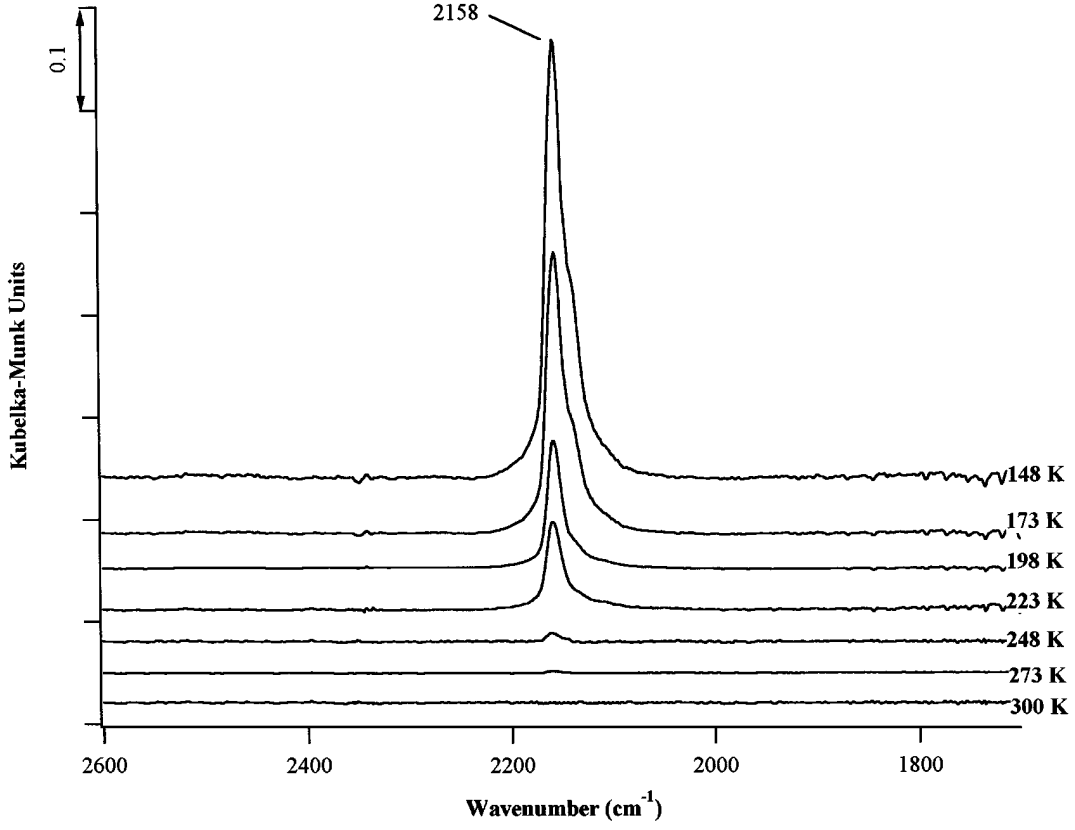


**FIG. 11.** DRIFT spectra of CO adsorbed at different temperatures on 4.9% $Cu/Al_2O_3$ calcined at 573 K.

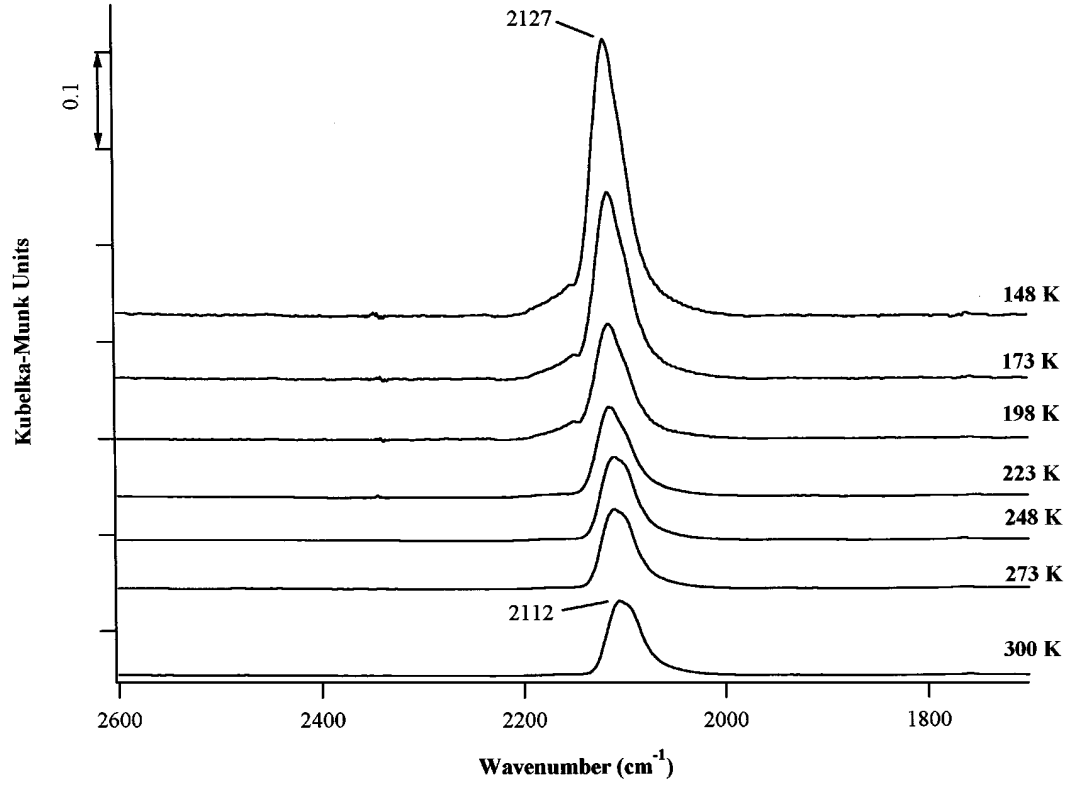


**FIG. 12.** DRIFT spectra of CO adsorbed at different temperatures on 4.9% $Cu/Al_2O_3$ reduced at 473 K.

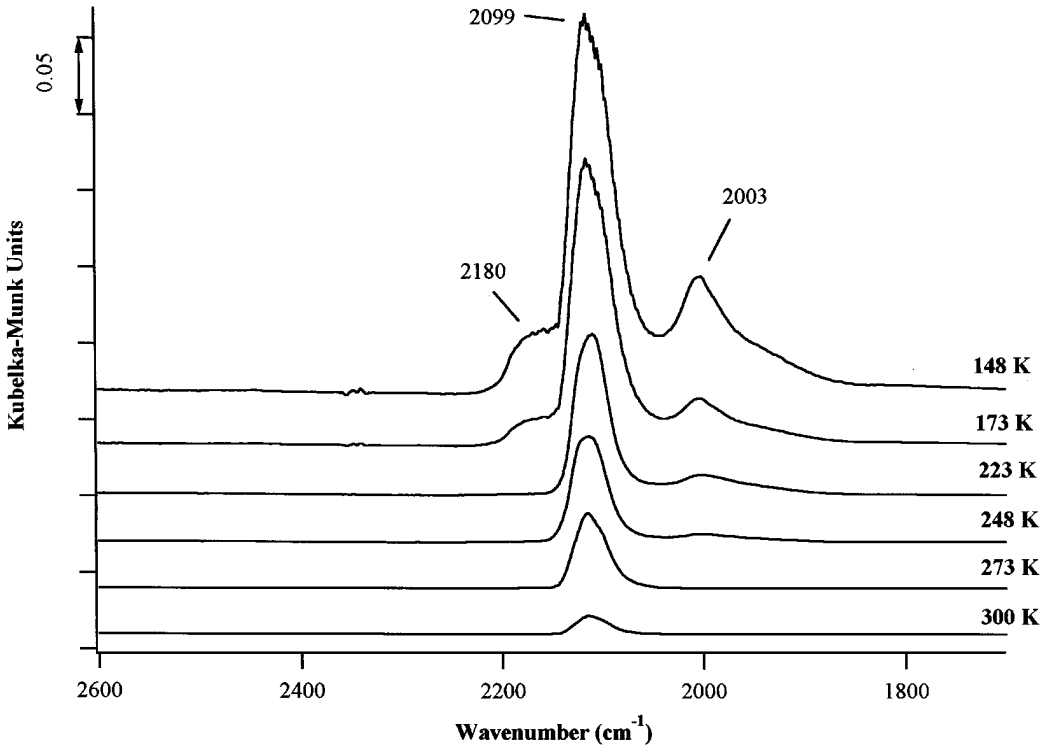


**FIG. 13.** DRIFT spectra of CO adsorbed at different temperatures on 4.9% $Cu/Al_2O_3$ reduced at 573K.

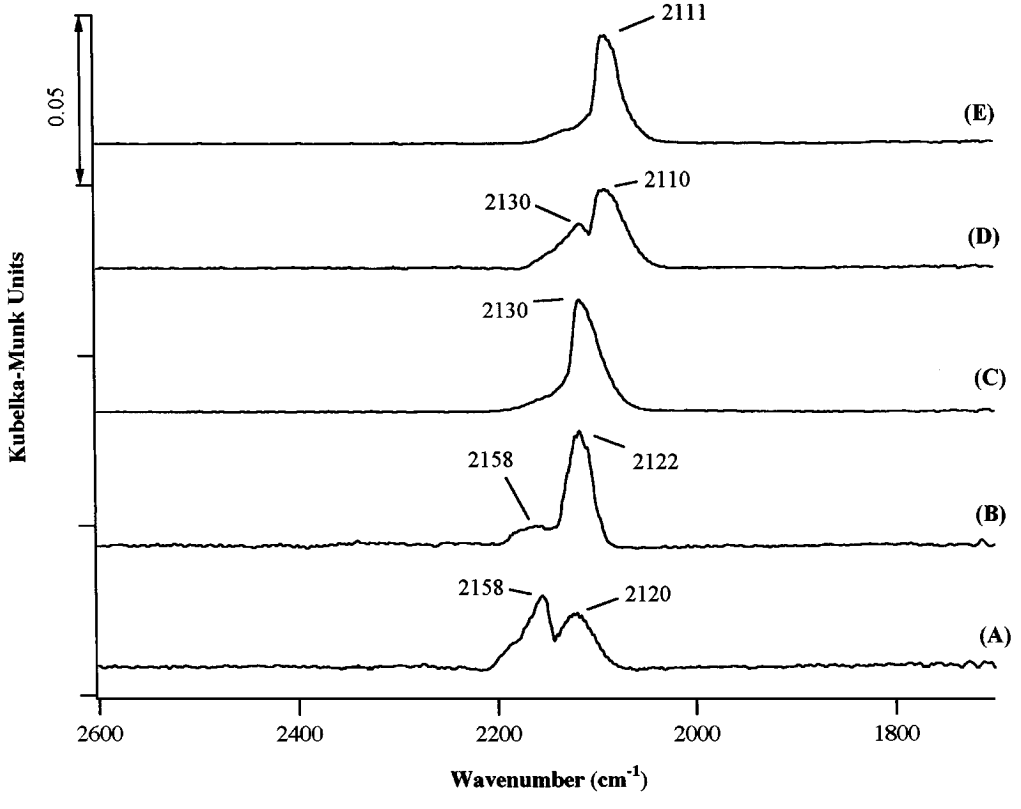


**FIG. 14.** DRIFT spectra of CO adsorbed at 173 K on 5% Cu/DM after (A) calcination at 423 K, and reduction at (B) 423 K, (C) 473 K, (D) 573 K, and (E) 673 K; $P_{CO} = 75$ Torr.

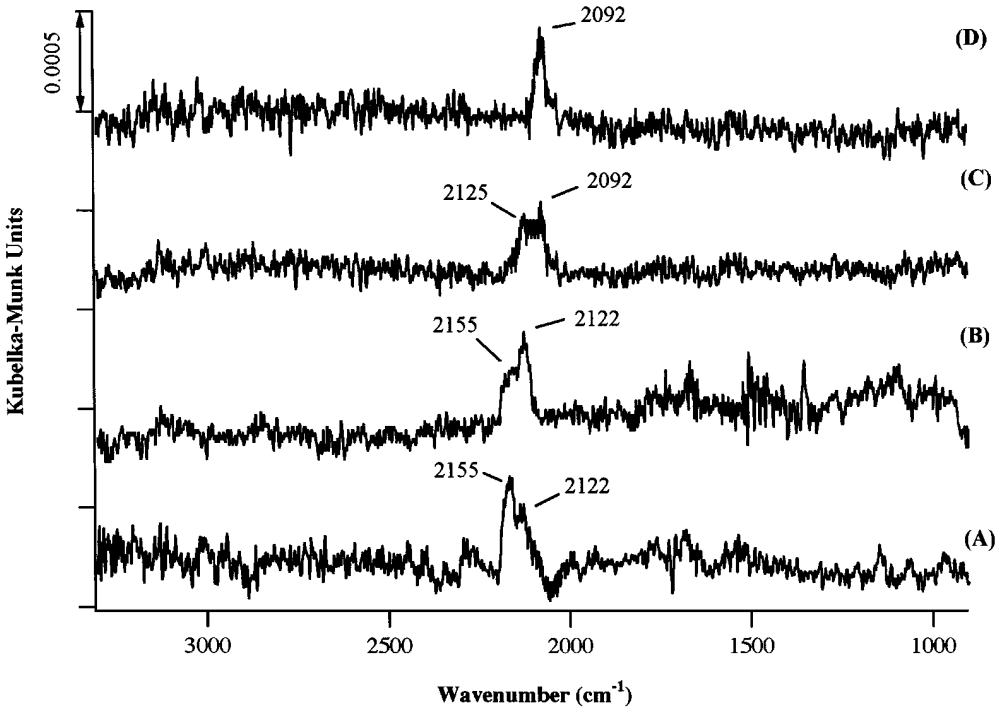


**FIG. 15.** DRIFT spectra of CO adsorbed at 173 K on 5.1% Cu/GF after (A) treatment in Ar at 423 K, and reduction at (B) 423 K, (C) 573 K, and (D) 673 K; $P_{CO} = 75$ Torr.

To further verify this literature-based assignment of bands between 2110 and 2120 $cm^{-1}$ to CO adsorbed on surface $Cu^{+1}$ species, fresh samples of each of the four catalysts discussed above, i.e., $Cu/SiO_2$, $Cu/Al_2O_3$, $Cu/TiO_2$, and Cu/DM, along with samples of $Cu/ZrO_2$ and Cu/GF, were loaded into the DRIFTS cell and reduced in flowing $H_2$ for 4 h at 573 K. The cell was purged and the temperature was decreased to 363 K; then the samples were exposed to a flowing mixture of 10% $N_2O$ in Ar for 30 min followed by an Ar purge for 1 h. This treatment has been shown to reoxidize all surface $Cu^0$ species to $Cu^{+1}$ species, resulting in a uniform surface comprised entirely of $Cu^{+1}$ sites (14). Following this, the standard procedure discussed previously was employed to obtain spectra after exposure to CO and purging in Ar which are shown as spectrum C in Figs. 3–6 and as spectra A and B in Fig. 7. These additional spectra exhibit bands at positions identical to those obtained after the reduction step; however, the intensity of these new bands is significantly enhanced, especially in the case of $Cu/TiO_2$, where the concentration of any $TiO_x$ species on the Cu surface after reduction should be decreased or eliminated (48). The irreversible CO and oxygen uptakes on these six catalysts, measured in the adsorption system after the same reduction–reoxidation treatment, are given in Table 1. Following the reoxidation by $N_2O$, in every case a huge increase in the amount of irreversible CO adsorption occurred, compared to that after reduction, while oxygen adsorption dropped to zero. These results verify the previous assignment of bands in this region.

These results further support the assignment of all bands between 2120 and 2110 $cm^{-1}$ only to CO irreversibly adsorbed on cuprous ions. The sharp drop in the irreversible CO uptake on these catalysts after the higher temperature reductions at 573 K is concurrent with an increase in the amount of oxygen adsorbed on these catalysts via $N_2O$ decomposition, whereas a significant increase in the CO uptake following the reduction–reoxidation step is synchronous with the drop in adsorbed oxygen to zero. This behavior is entirely consistent with the proposal that $N_2O$ decomposition at 363 K measures only the number of metallic Cu surface atoms, whereas irreversible CO adsorption at 300 K is proportional to the surface concentration of cuprous ions. The actual dispersion of Cu should be based on the amount of $N_2O$ decomposed and the amount of CO irreversibly chemisorbed, assuming that most of the $Cu^{+1}$ sites are covered at 300 K. Table 1 compares Cu dispersions estimated by the sum of CO + O uptakes based on the stoichiometry of Eq. [1], while Table 2 compares crystallite sizes obtained by TEM and XRD with those calculated from the adsorption results. For the $Cu/SiO_2$, $Cu/Al_2O_3$, and Cu/DM catalysts, the agreement between the values is much improved in all cases when both oxygen and CO adsorption are taken into account, even if there is some uncertainty about the relationship between crystallite size and dispersion for $Cu_2O$ and the manner in which these two phases coexist. For $Cu/TiO_2$ both the DRIFT spectra and the chemisorption data indicate that even after reduction at 473 K, most of the Cu surface is metallic;

hence consideration of the small amount of CO is not significant.

An examination of the subambient spectra shows that not only is the $Cu^{+1}$-CO band enhanced as the temperature decreases, but bands associated with the more weakly bound $Cu^{+2}$-CO and $Cu^0$-CO species are also retained and their intensity is very temperature dependent. The enhancement of the former band implies that CO adsorption at 300 K may underestimate $Cu^{+1}$ sites. The strong 2159 $cm^{-1}$ band obtained in the spectrum of calcined $Cu/SiO_2$ at 148 K in Fig. 8 can be readily assigned to a linear $Cu^{+2}$-CO complex. The assignment is justified not only on the basis of peak position, but also on the basis of weak binding, as evidenced by the absence of a residual peak at 300 K. The 2240 $cm^{-1}$ has been assigned to CO stabilized on isolated $Cu^{+2}$ ions in the $SiO_2$ matrix (38). The shoulder at 2130 $cm^{-1}$ lies in the region corresponding to $Cu^{+1}$-CO species, but the absence of any distinguishable features at 300 K indicates much weaker binding occurs, perhaps due to $Cu^{+1}$ sites being isolated in a CuO matrix. Alternatively, based on the work of Pritchard and co-workers, this shoulder might be assigned to CO adsorbed on a small fraction of densely packed low-index planes of CuO. In Fig. 9 the residual band at 2115 $cm^{-1}$ in the 300 K spectrum of $Cu/SiO_2$ reduced at 473 K is clearly attributable to $Cu^{+1}$-CO species, whose concentration increases and whose position shifts to 2117 $cm^{-1}$ as the adsorption temperature is lowered. The shoulder at 2149 $cm^{-1}$ is attributed to residual unreduced $Cu^{+2}$ ions. Similarly, the spectra in Fig. 10 for $Cu/SiO_2$ reduced at 573 K indicate almost complete reduction to $Cu^0$ because of the absence of residual bands at 300 K and the dominance of bands at 2107 and 2062 $cm^{-1}$ which can be attributed to CO on metallic Cu. The latter peak can occur on certain high index plances of Cu (21–24); however, it might also be due to very small Cu particles with enhanced electron densities in the hybrid d + s valence shells. The shoulder at 2160 $cm^{-1}$ may be due to very stable $Cu^{+2}$ ions embedded in the silica matrix.

The spectra for $Cu/Al_2O_3$ (Figs. 11–13), Cu/DM (Fig. 14), and Cu/GF (Fig. 15) can also be analyzed utilizing the same arguments. Whereas the 2158 $cm^{-1}$ peak in Fig. 11, obtained with calcined $Cu/Al_2O_3$ can be attributed to linear $Cu^{+2}$-CO complexes, the stable band at 2112 $cm^{-1}$ in the spectrum at 300 K for $Cu/Al_2O_3$ reduced at 473 K, which grows and shifts to 2127 $cm^{-1}$ at 148 K (Fig. 12), can be unambiguously attributed to linear $Cu^{+1}$-CO complexes. For $Cu/Al_2O_3$ reduced at 573 K (Fig. 13), the 2099 $cm^{-1}$ band can be assigned to a linear $Cu^0$-CO species, whereas bridged $Cu^0$-CO complexes can be held responsible for the low wavenumber band at 2003 $cm^{-1}$. On these very small (ca 1.2 nm) $Cu^0$ crystallites, some irreversible CO adsorption occurs at 300 K. As before, the 2180 $cm^{-1}$ band can be assumed to be due to isolated $Cu^{+2}$ cations or Cu clusters. In contrast to the spectra of calcined $Cu/SiO_2$ and $Cu/Al_2O_3$, the spectrum of calcined Cu/DM exhibits a prominent band at 2115 $cm^{-1}$ at 300 K (not shown), attributed to $Cu^{+1}$ species based on its position, as well as its presence at 300 K, which shifts to 2120 $cm^{-1}$ at 173 K, along with the appearance of another peak at 2158 $cm^{-1}$ at this temperature (Fig. 14). Thus, there is a mixture of $Cu^{+2}$ as well as $Cu^{+1}$ species on the surface of Cu/DM after this lower-temperature calcination step. As the reduction temperature increases to 473 K, $Cu^{+2}$ is converted almost completely to $Cu^{+1}$, as indicated by spectrum 14(C), reduction at 573 K gives a mixture of $Cu^{+1}$ and $Cu^0$, while reduction at 673 K produces mostly $Cu^0$ at the surface. The XRD results in Table 2 also indicate a mixture of $Cu_2O$ and metallic Cu after reduction at 573 K.

The signal-to-noise ratios obtained with Cu/GF samples were significantly lower than those achieved with the previous samples, as shown in Fig. 15, even after optimal dilution with $CaF_2$. Regardless, the trends are similar to those observed with the other catalysts and they demonstrate that C-supported Cu can also be studied with this technique. Although not calcined in $O_2$, the heat treatment in Ar at 423 K produced a mixture of $Cu^{+2}$ and $Cu^{+1}$ surface states, as shown in Fig. 15A, similar to that of the calcined Cu/DM sample. Reduction at progressively higher temperature showed an evolution of surface states from $Cu^{+2}$ to $Cu^{+1}$ to $Cu^0$, and after reduction at 673 K, only $Cu^0$ exists at the surface (Fig. 15D).

The spectra in this study have demonstrated that, based on their peak position in the infrared spectrum, as well as their relative binding strengths, it is possible to distinguish among CO species adsorbed on $Cu^{+2}$, $Cu^{+1}$, and $Cu^0$ sites. Although bands in the three different regimes of wavenumber can be detected at 300 K under sufficiently high CO pressures, the subambient spectra at 173 K or lower after removal of gas-phase CO are much better resolved. A comparison of the spectra obtained at 300 K and 173 K is provided in Fig. 16 for a $Cu/Al_2O_3$ sample reduced at 573 K. In the presence of 75 Torr CO, bands appear at 2099 and 2003 $cm^{-1}$ in the spectrum obtained at 173 K (Fig. 16A) along with a shoulder near 2180 $cm^{-1}$. As discussed earlier, these bands can be assigned to linear and bridge bonded CO on $Cu^0$ and linear CO on isolated $Cu^{+2}$ sites. In addition, two strong bands develop at 1657 and 1433 $cm^{-1}$. Based on similar spectra of CO adsorption on pure, unloaded $Al_2O_3$ pretreated in $H_2$ at 573 K for 4 h, these bands can be assigned to CO stabilized on $Al_2O_3$ as bidentate and noncoordinated carbonate species, respectively (19,49). Removal of CO by purging with Ar has little effect on any of these peaks at 173 K (Fig. 16B). Under 75 Torr CO at 300 K, bands corresponding to the two forms of CO on metallic Cu are visible at 2090 and 1998 $cm^{-1}$, along with those for CO adsorbed on the $Al_2O_3$ support (Fig. 16C). Purging with Ar removes all these bands, leaving only a very weak peak at 2105 $cm^{-1}$. Consequently, one can follow the transition in oxidation states of Cu in a given catalyst as reduction temperature varies by comparing the spectra of CO irreversibly adsorbed at 173 K on the pretreated catalysts, as demonstrated in Figs. 14 and 15. Similar

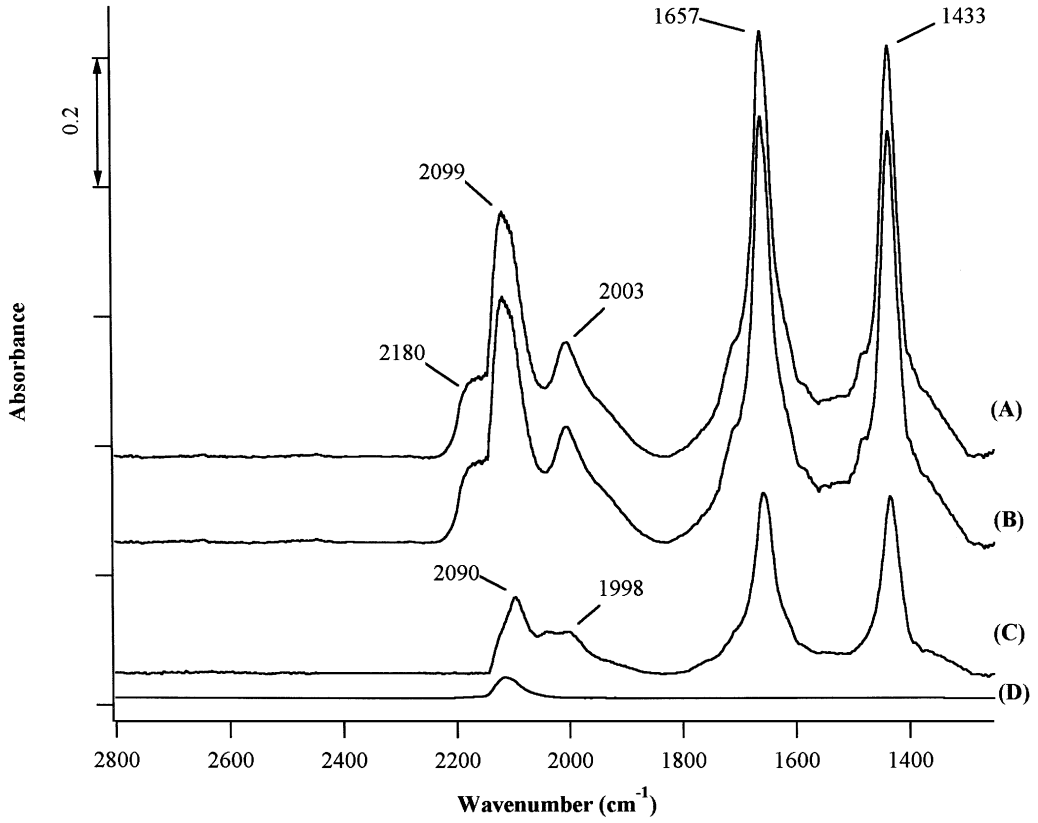


**FIG. 16.** DRIFTS spectra of CO adsorbed on 4.9% $Cu/Al_2O_3$ after reduction at 573 K for 4 h: (A) in presence of 75 Torr CO at 173 K; (B) after purging at 173 K; (C) in presence of 75 Torr CO at 300 K; and (D) after purging at 300 K.

representations of the progression of reduction as a function of the reduction temperature can be obtained from the spectra of Cu dispersed on the oxide supports. Consequently, this technique appears to be a universal, easily applied characterizational approach to determine the surface oxidation states of Cu. When combined with the $N_2O$ and room temperature CO adsorption measurements obtained in this study, the number of $Cu^{+1}$ and $Cu^0$ sites can be estimated. Another approach—subambient CO adsorption combined with DRIFTS spectra at the same temperature—can potentially provide a quantitative determination, assuming that the extinction coefficient for CO is similar on all three types of sites. However, the measurements would have to be done at an optimum temperature which is low enough to allow adsorption of CO on all three sites, yet high enough to minimize CO adsorption on the support materials. Additional complications like capillary condensation may also be encountered when dealing with microporous supports like activated carbon (48).

Some additional information can be obtained from the temperature dependence of the intensities illustrated in Figs. 8–13 and elsewhere (49). If adsorption on all three types of sites can be represented by a Langmuir isotherm, then heats of adsorption can be estimated in the low coverage region for CO on $Cu^0$ and $Cu^{+2}$ sites and in the high coverage region for CO on $Cu^{+1}$ sites. Figure 17A demonstrates that detectable amounts of CO on $Cu^0$ and $Cu^{+2}$ sites do not exist until temperatures drop below 300 and 250 K, respectively, whereas saturation appears to be approached at 148 K for CO on the $Cu^{+1}$ sites. In the former case, $\theta = I/I_O = KP_{CO}$, where $I_O$ is the intensity at saturation coverage, thus $\ell n\, I = \ell n\, I_O A + Q_{ad}/RT$, since $P_{CO}$ is constant at 75 Torr and the slope of $\ell n\, I$ or $\ell n(I_T/I_{148\,K})$ vs $1/T$ will yield $-\Delta H_{ad}/R$. At the much higher coverages that exist for the $Cu^{+1}$ sites, $\theta = I/I_O = KP_{CO}/(1 + K_{CO}P_{CO})$, where $I_O$ is assumed equal to $I$ at 148 K, and the appropriate plot to determine $Q_{ad}/R$ is $\ell n\,(\theta/1-\theta)$ vs $1/T$. These three plots for $Cu/Al_2O_3$ are represented in Fig. 17B, thus heats of adsorption of 4.2, 9.8, and 5.0 kcal/mole are obtained for CO adsorbed on $Cu^0$, $Cu^{+1}$, and $Cu^{+2}$ sites, respectively. Similar plots for $Cu/SiO_2$ and Cu/DM give similar values (49), all of which are listed in Table 4. The weaker bonding on $Cu^0$ and $Cu^{+2}$ sites is clearly evident. Values previously reported for the heat of adsorption of CO on Cu and Cu oxide surfaces, obtained using a variety of techniques, are also listed in Table 4 for comparison (49–62). The single earlier value for $Cu^{+2}$ sites is very consistent with those calculated here from the IR spectra. For $Cu^0$ surfaces, $Q_{ad}$ values between 5 and 15 kcal/mole have been determined over a wide temperature range of 77–493 K, while for $Cu^{+1}$ surfaces, $Q_{ad}$ values

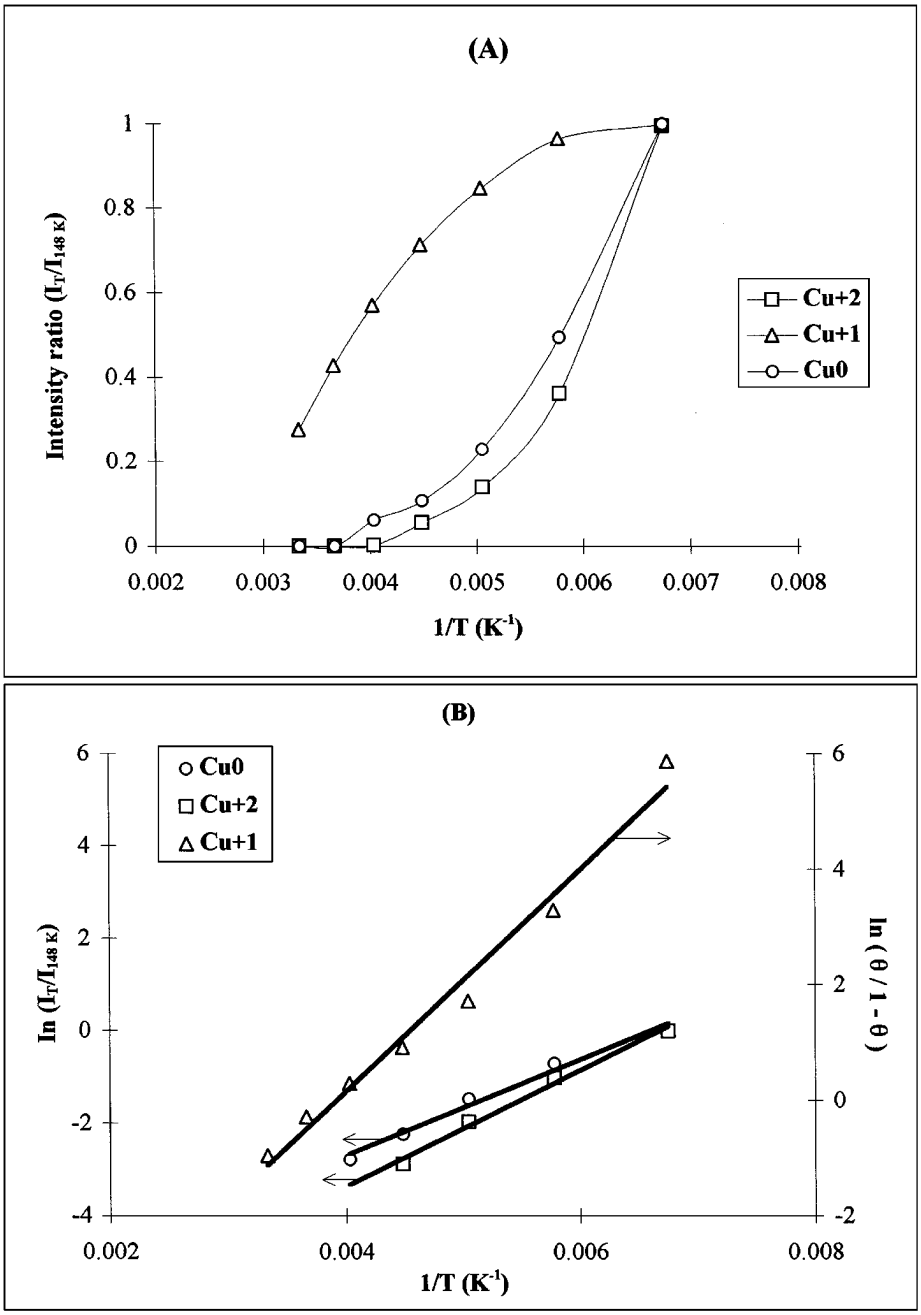


**FIG. 17.** (A) Variation in the K-M intensity of CO adsorbed on $Cu^0$, $Cu^{+1}$, and $Cu^{+2}$ as a function of temperature. (B) Arrhenius plots for heat of adsorption.

obtained over a similar temperature range fall between 5 and 22 kcal/mole. Thus for $Cu^0$ our values agree only with the low end previously reported, perhaps due to incomplete reduction, whereas our values for $Cu^{+1}$ are mid-range, compared to others. To summarize, from Table 4 average values for the heat of adsorption of CO on $Cu^0$, $Cu^{+1}$, and $Cu^{+2}$ can be calculated to be 4.7, 11.7, and 5.3 kcal/mole, respectively.

Finally, one can also address the applicability of DRIFTS to these systems in another quantitative way. The mathematical model developed by Kubelka and Munk for diffuse reflectance relates the concentration of the IR absorbing component of the sample and the scattered radiation intensity in the same manner as the Beer–Lambert law for transmission measurements (45,63–69). For an "infinitely thick" sample, the Kubelka–Munk function can be expressed as

$$f(R_\infty) = (1-R_\infty)^2/2R_\infty = \frac{k}{s} = \frac{2.303\,\varepsilon C}{s},$$

where $R_\infty$ is the diffuse reflectance spectrum of the infinitely thick sample proportional to that of a nonabsorbing background or reference, $k$ is the absorption coefficient, $\varepsilon$ is the extinction coefficient of the absorber, and $s$ is the

**TABLE 4**

**Heat of Adsorption of CO on Cu Sites**

| Site | Form | $Q_{ad}$ (kcal/mole) | Temp range (K) | Reference |
|---|---|---|---|---|
| $Cu^{+2}$ | $Cu/SiO_2$ | 6.9 | 358–493 | (29) |
| | $Cu/SiO_2$ | 7.0 | 148-300 | This study |
| | $Cu/\eta$-$Al_2O_3$ | 5.0 | 148-300 | This study |
| | Cu/DM | 3.8 | 148-300 | This study |
| $Cu^{+1}$ | $Cu/SiO_2$ | 4.7 | 358-493 | (29) |
| | $Cu/Al_2O_3$ | 16.9 | — | (50) |
| | $Cu/\eta$-$Al_2O_3$ | 7.2 | 300-413 | (30) |
| | Bulk $Cu_2O$ | 19.4 | 90-300 | (47) |
| | $Cu/SiO_2$ | 5.2 | 408-473 | (26) |
| | $Cu_2O$ film | 20 | — | (51) |
| | Bulk $Cu_2O$ | 20 | 300 | (52) |
| | $Cu_2O(100)$ | 16.7 | 120-700 | (53) |
| | Cu/ZSM-Y | 14.7 | 370-503 | (54) |
| | Cu/ZnO | 22.4 | — | (55) |
| | Cu/ZnO | 12-18 | 123-400 | (56) |
| | Cu/ZnO | 17.0 | 303 | (61) |
| | $Cu/SiO_2$ | 13.2 | 148-300 | This study |
| | $Cu/\eta$-$Al_2O_3$ | 9.8 | 148-300 | This study |
| | Cu/DM | 12.2 | 148-300 | This study |
| $Cu^0$ | $Cu/SiO_2$ | 5.2 | 358-493 | (29) |
| | Cu(100) | 14.5 | 77-195 | (20) |
| | Cu(110) | 14.5 | 90-250 | (57) |
| | Cu(311) | 5.2-14.5 | 77-300 | (58) |
| | $Cu/SiO_2$ | 14.5 | 447-472 | (59) |
| | Cu/Film | 9.3 | 195-288 | (60) |
| | CuZnO | 9.6 | 303 | (61) |
| | Cu(111) | 11.7 | 188-198 | (62) |
| | $Cu/SiO_2$ | 4.8 | 148-300 | This study |
| | $Cu/\eta$-$Al_2O_3$ | 4.2 | 148-300 | This study |
| | Cu/DM | 5.2 | 148-300 | This study |

**TABLE 5**

**Slopes from Fig. 18 (2.303 $\varepsilon/s$) and Scattering Coefficients ($s$) for CO on Supported Copper Catalysts ($T_{red} = 200°C$)**

| Catalyst (5 wt% Cu) | $2.303\ \varepsilon/s \times 10^{-4}$ ($cm^3/\mu mol$) | $s \times 10^{3a}$ ($cm^{-1}$) |
|---|---|---|
| Cu/DM | 1.1 | 6.2 |
| $Cu/SiO_2$ | 3.9 | 1.8 |
| $Cu/Al_2O_3$ | 7.8 | 0.9 |
| $Cu/TiO_2$ | 6.8 | 1.0 |

[a] Based upon $\varepsilon = 0.3\ cm^2/\mu mol$ [32].

scattering coefficient of the sample matrix. Experimental parameters which can lead to deviations from a linear relationship between intensity and concentration have been discussed previously (45); however, over a certain range of concentration, a linear relationship should exist between the peak intensity of the Kubelka–Munk function, $f(R_\infty)$, at a given frequency and the concentration $C$, with a zero $y$-intercept occurring if the scattering coefficient $s$ remains constant for a given sample. Based on the uptakes measured in Table 1 for four catalysts, the spectra in Figs. 3–6 do indeed fulfill this relationship when represented in Kubelka–Munk intensities, as shown in Fig. 18. It is known that $s$ can depend strongly on the matrix material surrounding the absorber (69), and an estimate of the values of $s$ can be made if the extinction coefficient, $\varepsilon$, is known. If a value of $\varepsilon = 0.3\ cm^2/\mu mol$ is chosen for CO adsorbed on $Cu^{+1}$ (19) and assumed to be independent of concentration, the values of $s$ estimated from the slopes, $2.303\ \varepsilon/s$, in Fig. 18 are listed in Table 5. The scattering coefficients for the

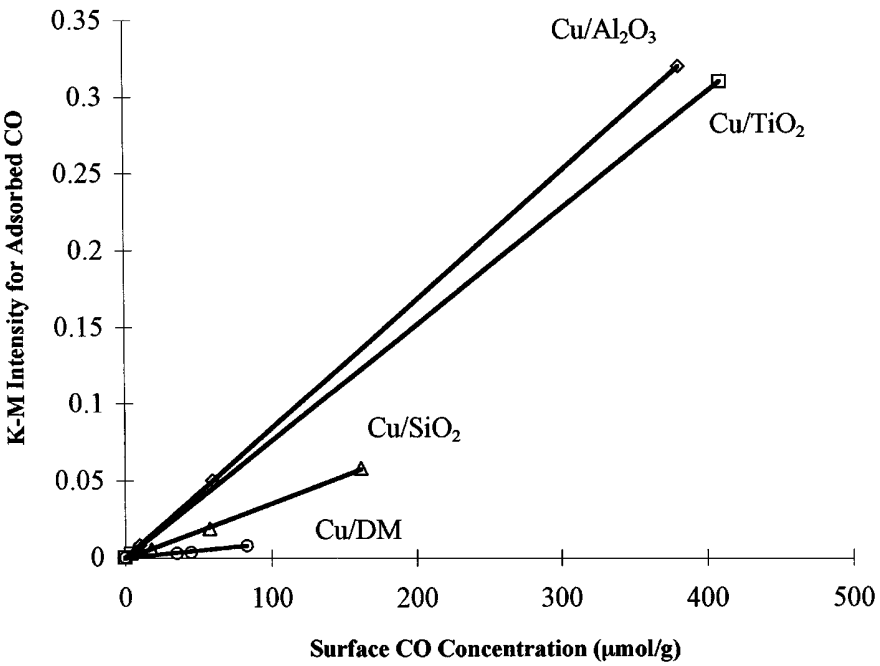


**FIG. 18.** Variation in the K-M intensity of CO adsorbed on $Cu^{+1}$ at 300 K as a function of $Cu^{+1}$ surface concentration.

three oxide supports are not too different and fall in the range of $0.9–1.8 \times 10^{-3}$ $cm^{-1}$; however, that for the much more transparent diamond is significantly higher. It is possible that some of this variation is due to the difference in Cu (or $Cu_2O$) crystallite sizes.

## SUMMARY

Cu catalysts obtained by dispersing Cu on a variety of supports including $SiO_2$, $Al_2O_3$, $TiO_2$, $ZrO_2$, synthetic diamond powder and graphitized carbon fibers, were characterized by CO chemisorption, $N_2O$ decomposition, TEM, XRD, and DRIFTS spectra of CO adsorption at 300 K as well as at sub-ambient temperatures. Dispersions of Cu, considering both the O uptake via $N_2O$ decomposition at 363 K to measure $Cu^0$ sites and the irreversible CO uptake at 300 K to measure $Cu^{+1}$ sites, were found to give the best agreement with the TEM and XRD data. Using a technique based on DRIFT spectra of CO adsorbed on these catalysts at subambient temperatures (down to 148 K), the transition in the oxidation state of Cu can be followed as a function of reduction temperature. This IR technique appears to be a universal, easily applied characterizational approach to determine the surface oxidation states in supported Cu catalysts. Heats of adsorption for CO on $Cu^0$, $Cu^{+1}$, and $Cu^{+2}$ sites, determined on the basis of the intensities of the subambient DRIFT spectra, are consistent with values reported in the literature.

## ACKNOWLEDGMENTS

Support for this project was provided by the National Science Foundation under Grant CTS-9415335. TEM work was conducted in the electron microscopy facility of the Materials Characterization Laboratory at Pennsylvania State University.

## REFERENCES

1. Mehta, S., Simmons, G. W., Klier, K., and Herman, R. G., *J. Catal.* **57**, 339 (1979).
2. Monnier, J. R., Apai, G., and Hanrahman, M. J., *J. Catal.* **88**, 523 (1984).
3. Burch, R., Golunski, S. E., and Spencer, M. S., *J. Chem. Soc. Faraday Trans.* **88**, 523 (1984).
4. Hubaut, R., Daage, M., and Bonnelle, J. P., *Appl. Catal.* **22**, 231 (1986).
5. Chudinov, M. G., Kuznetsov, B. N., Alekseev, A. M., and Pak, G. P., *Kinet. Catal.* **29**, 590 (1988).
6. Pillai, R. B. C., *Catal. Lett.* **26**, 365 (1994).
7. Nishimura, E., Inoie, Y., and Yasumori, I., *Bull. Chem. Soc. Jpn* **48**, 803 (1975).
8. Capece, F. M., Castro, V. D., Furlani, C., Mattogno, G., Fragale, C., Gargano, M., and Rossi, M., *J. Elec. Spec. Rel. Phenom.* **27**, 119 (1982).
9. Imura, A., Inoie, Y., and Yasumori, I., *Bull. Chem. Soc. Jpn* **56**, 2203 (1983).
10. Makarova, O. V., Yur'eva, T. M., Kustova, G. N., Ziborov, A. V., Plyasova, L. M., Miyukova, T. P., Davydora, L. P., and Zaikovskii, V. I., *Kinet. Catal.* **34**, 863 (1993).
11. Dandekar, A., Rao, R., Baker, R. T. K., and Vannice, M. A., *J. Catal.* **171**, 406 (1997).
12. Leon y Leon, C. A., and Vannice, M. A., *Appl. Catal.* **69**, 269 (1991).
13. Dell, R. M., Stone, F. S., and Tiley, P. F., *Trans. Faraday Soc.* **49**, 195 (1953).
14. Scholten, J. J. F., and Konvalinka, J. A., *Trans. Faraday Soc.* **65**, 2465 (1969).
15. Bruce, M. I., *J. Organometal. Chem.* **44**, 209 (1972).
16. Huang, K. H., *J. Mol. Catal.* **64**, 85 (1991).
17. Hollins, P., *Surf. Sci. Rep.* **16**, 51 (1992).
18. Amores, G. M. G., Sanchez-Escribano, V., Busca, G., and Lorenzello, V., *J. Mater. Chem.* **41**, 965 (1994).
19. Davydov, A. A., "Infrared Spectroscopy of Adsorbed Species on the Surface of Transition Metal Oxides," Wiley, London, 1990.
20. Pritchard, J., *J. Vac. Sci. Tech.* **9**, 895 (1971).
21. Prichard, J., Catterick, T., and Gupta, R. K., *Surf. Sci.* **53**, 1 (1975).
22. Horn, K., Hussain, M., and Pritchard, J., *Surf. Sci.* **63**, 244 (1977).
23. Horn, K., and Pritchard, J., *Surf. Sci.* **55**, 701 (1976).
24. Hollins, P., and Pritchard, J., *Surf. Sci.* **134**, 91 (1983).
25. London, J. W., and Bell, A. T., *J. Catal.* **31**, 32 (1973).
26. London, J. W., and Bell, A. T., *J. Catal.* **31**, 86 (1973).
27. Kavtaradze, N. N., and Sokolova, N. P., *Russ. J. Phys. Chem.* **44**, 603 (1970).
28. Busca, G., *J. Mol. Catal.* **43**, 225 (1987).
29. Kohler, M. A., Cant, N. W., Wainwright, M. S., and Trimm, D. L., *J. Catal.* **117**, 188 (1989).
30. Choi, K. I., and Vannice, M. A., *J. Catal.* **131**, 22 (1991).
31. Padley, M. B., Rochester, C. H., Hutchings, G. J., and King, F., *J. Catal.* **148**, 438 (1994).
32. Pestryakov, A. N., and Davydov, A. A., *Kinet. Katal.* **37**, 859 (1996).
33. Boccuzzi, F., and Chiorino, A., *J. Phys. Chem.* **100**, 3617 (1996).
34. Hadjivanov, K. I., Kantcheva, M. M., and Klissurski, D. G., *J. Chem. Soc. Faraday Trans.* **92**, 4595 (1996).
35. Aubke, F., and Wang, C., *Coord. Chem. Rev.* **137**, 483 (1994).
36. Lokhov, T., and Davydov, A., *Kinet. Katal.* **20**, 1498 (1979).
37. Hadjivanov, K. I., Kantcheva, M. M., Klissurski, D. G., and Davydov, A. A., *J. Chem. Soc. Faraday Trans.* **87**, 907 (1991).
38. De Jong, K. P., Geus, J. W., and Joziasse, J., *J. Catal.* **65**, 437 (1980).
39. De Jong, K. P., Geus, J. W., and Joziasse, J., *Applica. Surf. Sci.* **6**, 273 (1980).
40. Gardner, R. A., and Petrucci, R. H., *J. Amer. Chem. Soc.* **19**, 776 (1978).
41. Balkenende, A. R., van der Grift, C. J. G., Meulenkamp, E. A., and Geus, J. W., *Appl. Surf. Sci.* **68**, 161 (1993).
42. Eischens, R. P., Pliskin, W. A., and Francis, S. A., *J. Chem. Phys.* **22**, 1786 (1954).
43. Seanor, D. A., and Amberg, C. H., *J. Chem. Phys.* **42**, 2967 (1965).
44. Venter, J. J., and Vannice, M. A., *Appl. Spect.* **42**, 1096 (1988).
45. Venter, J. J., and Vannice, M. A., *Carbon* **26**, 889 (1988).
46. Fanning, P. E., and Vannice, M. A., *Carbon* **31**, 721 (1993).
47. Garner, W. E., Stone, F. S., and Tiley, P. F., *Proc. Roy. Soc. Lond.* **211**, 472 (1952).
48. Haller, G. L., and Resasco, D. E., *Adv. Catal.* **36**, 173 (1989).
49. Dandekar, A., Ph.D. thesis, Pennsylvania State University, 1998.
50. Efremov, A. A., Pankratiev, Y. D., Davydov, A. A., and Boreskov, G. K., *React. Kinet., Catal. Lett.* **20**, 87 (1982).
51. Stone, F. S., *Adv. Catal.* **13**, 1 (1962).
52. Lokhov, Y. A., Sadykov, V. A., Tikhov, S. F., and Popovskii, V. V., *Kinet. Catal.* **26**, 152 (1985).
53. Cox, D. F., and Schulz, K. H., *Surf. Sci.* **249**, 138 (1991).
54. Huang, Y. Y., *J. Catal.* **30**, 187 (1973).
55. Baetzold, R. C., *J. Phys. Chem.* **89**, 4150 (1985).
56. Roberts, D. L., and Griffin, G. L., *Surf. Sci.* **19**, 298 (1984).
57. Ahner, J., Mocuta, D., Ramsier, R. D., and Yates, J. T., Jr., *J. Chem. Phys.* **105**, 6553 (1996).

58. Papp, H., and Pritchard, J., *Surf. Sci.* **53**, 371 (1975).
59. Monti, D. M., Cant, N. W., Trimm, D. L., and Wainwright, M. S., *J. Catal.* **100**, 17 (1986).
60. Trapnell, B. M. W., *Proc. Roy. Soc. Lond.* **218**, 566 (1953).
61. Fubini, B., Bolis, V., and Giamelo, E., *Thermochim. Acta* **85**, 23 (1985).
62. Kessler, J., and Thieme, F., *Surf. Sci.* **67**, 405 (1977).
63. Kubelka, P., and Munk, F. Z., *Tech. Phys.* **12**, 593 (1931).
64. Kubelka, P., *J. Opt. Soc. Am.* **38**, 448 (1948).
65. Kortrum, G., "Reflectance Spectroscopy: Principles, Methods and Applications," Springer-Verlag, New York, 1969.
66. Brimmer, P. J., and Griffiths, P. R., *Anal. Chem.* **58**, 2179 (1986).
67. Fraser, D. J. J., and Griffiths, P. R., *Appl. Spectrosc.* **44**, 193 (1990).
68. White, R. L., *Anal. Chem.* **64**, 2010 (1992).
69. Fuller, M. P., and Griffiths, P., ACS FTS/IR Notes, No. 27, June 1979.